# MOUNTAIN BIKE REAR SUSPENSION DESIGN: UTILIZING A MAGNETORHEOLOGICAL DAMPER FOR ACTIVE VIBRATION ISOLATION AND PERFORMANCE

A thesis proposal presented to the faculty of the Graduate School of
Western Carolina University in partial fulfillment of the
Requirements for the degree of Master of Science in Technology

By: Jacob R. Friesen

Advisor: Dr. Scott Pierce
School of Engineering + Technology

Committee Members:

Dr. Sudhir Kaul, School of Engineering + Technology
Dr. Wesley Stone, School of Engineering + Technology

May 2020

# ACKNOWLEDGEMENTS

First and foremost, I would like to thank my wife for her support. Without you, I would not have been able to relax when home or have a life outside of my education. You have supported and helped in every way possible.

I would like to thank my parents for their support. Without them, I wouldn't be where nor whom I am today. You have raised me to go after my passions and dreams while keeping the necessities in mind. There are no words or actions I can say or do to show the gratitude you deserve.

I would like to thank my fellow graduate student who has participated on this endeavor. Evens Morgan- Your skills in the machine shop and in the engineering field allowed me to relax while working on this because I knew I could count on you to help in any way.

Lastly, I would like to thank my thesis committee for their support throughout my graduate education. Dr. Scott Pierce- Without your passion for mountain biking and this experiment, I would not have had as much fun and laughter. Also, your knowledge and support have helped me accomplish all of this, thank you. Dr. Sudhir Kaul- The skills and knowledge about vibration analysis you have taught me, will help in my success of being an engineer, thank you. Dr. Wes Stone- Your support and guiding me to talk with the right people has advanced my knowledge in the outdoor economy.

TABLE OF CONTENTS

LIST OF TABLES

LIST OF FIGURES

ABSTRACT

MOUNTAIN BIKE REAR SUSPENSION DESIGN: UTILIZING A MAGNETORHEOLOGICAL DAMPER FOR ACTIVE VIBRATION ISOLATION AND PERFORMANCE

Jacob R. Friesen, M.S.T.

Western Carolina University (April 17, 2020)

Director: Dr. Scott Pierce

The introduction of suspension systems to mountain bikes began in the late 1980's and early 1990's. These suspensions created two types of mountain bikes; the hardtail and the full suspension mountain bike. However, designers of full suspension bikes must balance the need for pedaling efficiency, which calls for a stiff suspension, with comfort and trail contact, which calls for a soft suspension. This thesis presents experimental and theoretical results from the development of a rear suspension system that has been designed for a mountain bike. A magnetorheological (MR) damper is used to design a rear suspension system that can balance the need of ride comfort through shock absorption and performance characteristics such as handling and pedaling efficiency by using active control. Two control algorithms have been tested in this study – on/off control and proportional control. The damping was adjusted by setting the damper current to different levels in order to measure the effects of the change in response of the bike. The rear suspension system has been integrated into an existing bike frame and tested on a shaker table as well as a mountain trail. Shaker table testing demonstrates the effectiveness of the damper, while the trail testing indicates that the MR damper-based shock absorber can be used to

implement different control algorithms. The shaker table and trail testing results indicate that active damping control can be implemented using an MR damper. Using the results of these experimental tests, a theoretical test was simulated using a mathematical model; which was used to represent the mountain bike mounted to the shaker table. The results were plotted using transmissibility, power spectrum density, and frequency mode shape plots which indicated three applicable natural frequencies near 5, 9, and 10 Hz, when applying the mountain bike, rear suspension system, and rider weight/distribution used for this experiment. Upon the analysis using MATLAB, the mathematical model was determined to correctly represent the overall dynamics of the bicycle pertaining to the sprung mass. Additional accelerometers will need to be placed throughout the bicycle to determine if the mathematical model correctly represented the overall dynamics of the bicycle as a whole.

Keywords: mountain bike, magnetorheological damper, rear suspension.

# CHAPTER ONE: INTRODUCTION

This chapter contains an overview of this research as well as contextual information about magnetorheological dampers. A problem statement and outline of this study have been included in this chapter. This chapter also presents the motivation behind this research and its potential importance to the implementation of a magnetorheological (MR) damper into a rear suspension of a mountain bike.

## 1.1 Magnetorheological Dampers - Introduction

Magnetorheological (MR) dampers are hydraulic dampers that are filled with magnetorheological fluid. When the MR fluid is exposed to a magnetic field, the apparent viscosity of the fluid and the damping coefficient of the hydraulic damper is altered. This makes it possible to vary the damping coefficient of the MR damper by varying the strength of the magnetic field. This can be done by varying the current through an electromagnetic coil that is located near the fluid. This unique characteristic of the MR fluid has been used to implement semi-active damping in a number of different applications.

MR fluids consist of micron-sized ferromagnetic particles suspended in a carrier fluid [1]. When the fluid is exposed to a magnetic field, as seen in Figure [1.1], the ferromagnetic particles align themselves with the lines of flux of the magnetic field, which results in an increase in the apparent viscosity of the fluid. This results in an increase in the damping coefficient of the hydraulic damper. In the absence of a magnetic field the MR damper acts as a passive damper and the MR fluid is in its least viscous state. However, when a magnetic field is present, the MR damper becomes an active damper with the MR fluid in a semi-solid state. The semi-solid state and yield stress of the fluid depend upon the magnetic field. As the field strength increases the

fluid will eventually reach its “saturation point,” at which the fluid reaches its maximum viscosity. When the magnetic field applied to the MR fluid is removed, the fluid returns to its free-flowing state; meaning the viscosity of MR fluids is reversible. The MR fluid can be used in three different modes: shear mode - in which fluid flows between two parallel surfaces, flow mode or valve mode - in which fluid flows through an orifice, and squeeze mode - in which the fluid is put into compression between two parallel plates [2].

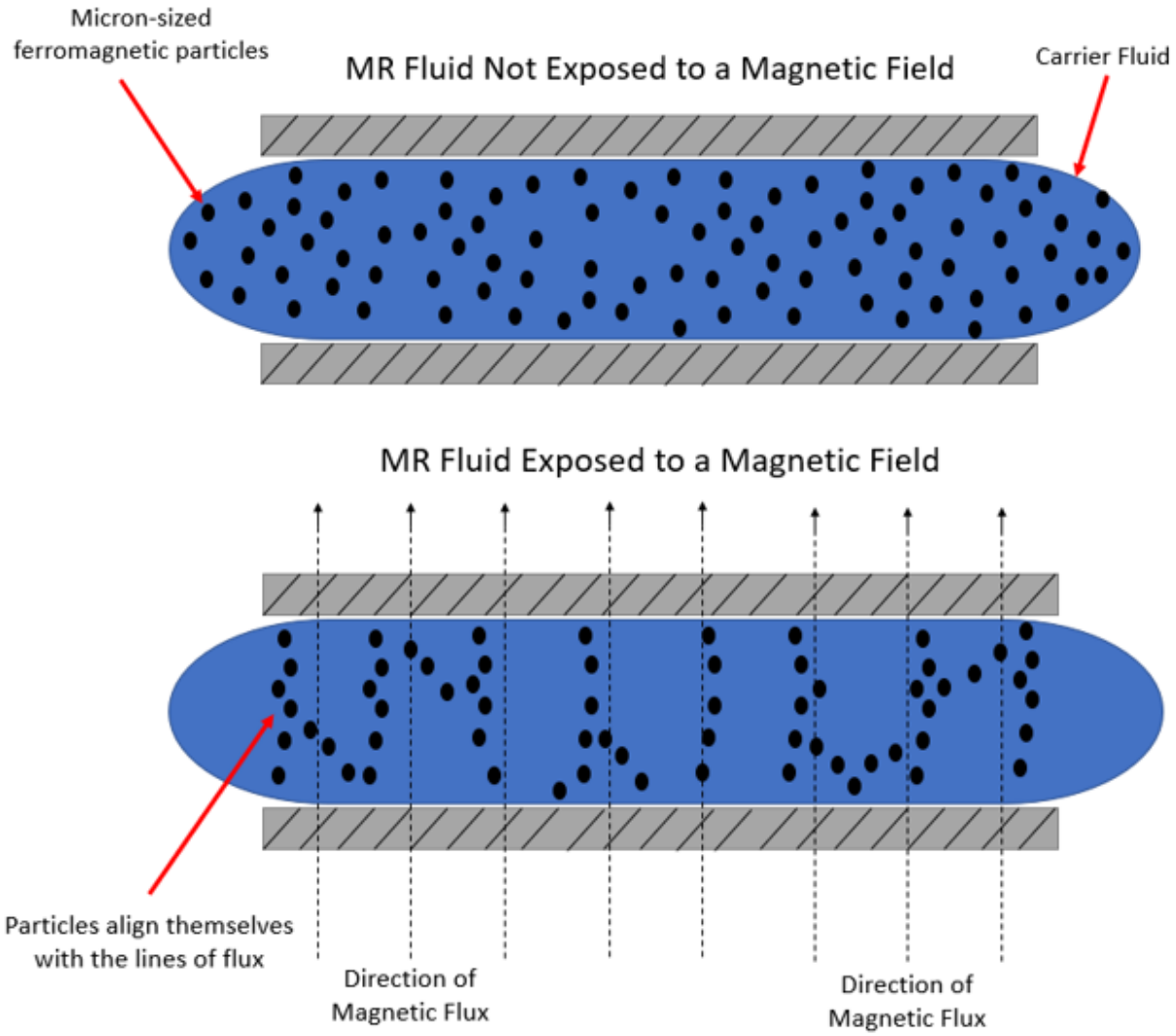


*Figure 1.1 - MR fluid exposed to a magnetic field*

Piston-based dampers such as the one used in this work, typically use the flow mode. The dampers work by passing the MR fluid from one chamber to another via orifices in a piston. A coil of wire located near the orifices generates a magnetic field within the orifices when a current is applied. The effective viscosity and damping coefficient change as the current through the coil is varied.

A wide range of industries use MR dampers and MR fluids in their products; such as, automotive, mechanical engineering, military and defense, and health industries. However, the applications of MR dampers and MR fluids have been limited because of their low shear strength. The automotive industry applies MR dampers mainly as active damping for the suspension systems as well as to the seating to support the rider and reduce the shock delivered to the riders' spine. Mechanical engineering has been developing stand-alone seismic dampers which will be able to absorb shock and oscillations within a structure in hopes to make them earthquake resistant. The military has been developing the MR fluid to make bullet proof vests. Finally, the medical and health industries have been using MR dampers for human leg prosthetics.

## 1.2 Scope of Thesis

A review of the literature pertaining to mountain bike rear suspension reveals that currently available active rear-suspensions only utilize on-off control methods. In these systems, the rear shock is maintained in a stiff condition until the bike hits a large bump, then the shock is switched to the softest possible condition. This study seeks to explore the use of an MR damper-based rear shock that can be used in a proportional-response mode. Research questions to be addressed are:

1. Can a mountain bike rear shock absorber be designed to utilize a MR damper with a control algorithm that is more complex than a simple on-off controller?
2. How does changing the shock control algorithm affect the performance of the mountain bike?
3. Can a mathematical model be formulated that captures the dynamics of the mountain bike?

The main goal of this study is to determine if the MR damper can be used in its semi-solid state, such that the control algorithm can be more than an on-off controller, as well as if the use of an MR damper on a mountain bike will be effective in reducing the accelerations felt by the rider at the saddle. The results of this study are expected to assist in understanding the use of MR dampers in the rear suspension system of a mountain bike.

### 1.3 Overview of Thesis

This thesis seeks to answer the research questions stated above by performing a series of tests at different parameters and testing methods (shaker table vs. trail). The parameters investigated in this study are the input frequency, which was varied during shaker table testing, and the current input to the damper, which was varied for both the shaker table and trail testing. The set frequencies were 2, 5, 10, and 20 Hz as well as a sine sweep of 1 - 20 Hz over 20 seconds. Each input frequency condition was run at damper currents of 0.0 A, 0.4 A, and 1.4 A. The range of values for the set frequencies were determined from literature [3, 4, 5, 6, 7]. The damper current values were determined from experimental methods discussed in Chapter 3.

The next chapter provides a literature review of contextual information about mountain bikes, rear suspensions, and MR dampers and fluids. This chapter also discusses other studies

that are relevant to the research done for this study including experimental set-ups and mathematical models. Chapter 3 discusses the experimental set-ups used for this study as well as the mathematical model built to represent the mountain bike on the shaker table. Chapter 4 displays the results from the shaker table and trail tests as well as the mathematical model. Chapter 5 discusses the results that were found in Chapter 4 and how they compare with the relevant studies. Chapter 6 draws an overall conclusion and provides some directions for future research.

# CHAPTER TWO: LITERATURE REVIEW

This chapter provides an overview of the literature related to this study to provide contextual information in support of the multiple aspects of research related to the content of this thesis. The first section provides a review of the history of bicycles, this includes the main types and styles of bicycles and the different types of rear suspension systems. Since this study primarily investigates the rear suspension of a dual suspension mountain bike, the other sections provide a background to magnetorheological dampers - including the properties, parameters and applications of the MR damper, vibration analysis, and designs of bicycle vibration analysis experiments. Finally, some examples of MR dampers used on bicycles is discussed.

## 2.1 History of Mountain Biking

The concept of mountain biking, "riding bicycles off-road, often over rough terrain" has been in practice since the early times of cycling. However, the sport of mountain biking started in the 1970's when cyclists began to race recreational bicycles on mountain trails [8]. In the 1980's, bicycle manufacturers began to design and manufacture bikes specifically for mountain biking, and in the 1990's the first modern bicycle suspensions started being incorporated into mountain bike designs. Since then, mountain biking has grown into a global phenomenon and has become one of the two major genres of cycling (road cycling and mountain biking). Commercial bicycles designed specifically for mountain biking come in many different types which cater to a specific riding style such as downhill riding, cross country racing, etc. One of the main differences between these different types of bikes is the style of the bicycle suspension. The biggest differentiator between suspension systems is whether the suspension is a front-only (hardtail) suspension or a full suspension.

### 2.1.1 Hardtail Vs. Full Suspension

With the rigorous terrains that mountain biking presents, mountain bikes utilize one or two suspension systems to reduce the excitation felt by the rider. These two suspension systems are a front suspension only, commonly referred to as a “hardtail” bike, or a dual system consisting of the front and rear shock absorbers, commonly referred to as a “full suspension” bike. The purpose of the front suspension is to absorb impacts from the front wheel. To do this, the front suspension of either design almost always consists of a pair of parallel, translational joints incorporated into the two fork tubes. These joints utilize some combination of mechanical springs, gas springs, and hydraulic dampers. This design most often contains an independently-adjustable compression and rebound response.

The rear suspension is designed to absorb impacts from the rear wheel. The rear suspension system of a mountain bike typically utilize a rear triangle that holds the rear wheel axle, which can pivot relative to the main frame tubes. The rear triangle consists of five parts: the frame, seat stay (link between the rear axle and rear suspension pivot), chain stay (link between the rear axle and the frame near the bottom bracket), rear suspension pivot (link connecting the frame, seat stay, and rear shock by pivot joints and pivoting about the frame pivot joint), and shock absorber. Motion of the rear triangle is controlled through a kinematic linkage (seat stay, chain stay, rear suspension pivot) and a shock absorber. The linkage geometry and the location of the shock absorber varies with the intended application and the design adopted by the bike manufacturer. Like the front system, rear shock absorbers typically consist of some combination of mechanical springs, air springs, and hydraulic dampers, often with independent compression and rebound control. Using a rear suspension system offers two primary advantages:

1) The rider experiences lower impact forces when travelling over rough terrain, thereby reducing rider fatigue.
2) The rear wheel of the bike maintains contact with the trail as it travels over a bump, resulting in improved handling.

### 2.1.2 Types of Rear Suspensions

Unlike front suspensions, rear suspension designs vary significantly from one manufacturer to another. This is due to the need to find a balance between high pedaling efficiency, which calls for a stiff suspension, with comfort and trail contact, which calls for a soft suspension. Furthermore, experienced riders desire a suspension with a highly customizable response that can be tuned for different riding styles and conditions. In order to meet these requirements, manufacturers have started to design bikes with semi-active suspension systems. The first such design became commercially available in 2002 with a suspension that uses a hydraulic inertia valve that is mounted on the rear triangle, near the rear axle. The default set up for the bike and hydraulic inertia valve is to be at its stiffest setting. When the rear wheel is excited by a bump or rough terrain, the inertia valve opens so that fluid can flow between the reservoir in the valve and a hydraulic damper in the rear shock absorber. This reduces the damping coefficient and makes the rear suspension become softer. Once the bump or rough terrain has been traversed, the suspension returns to the default setting [1].

A more recent design, which became commercially available in 2018, utilizes electronic sensors, actuators, and a controller powered by a battery [9]. Acceleration levels of the bike at the rear axle, seat tube, and front fork crown are measured using micro-electromechanical (MEMS) accelerometers mounted at these points. Accelerometer signals are sent to an onboard microcontroller which can change the damping characteristics of the rear shock absorber by

using a servo-controlled valve. This system can detect different combinations of acceleration conditions (e.g. accelerations that correspond to being airborne after a jump) and set the rear shock absorber to a soft or stiff setting.

One approach to semi-active damping of mountain bike suspensions that was developed in the 2000's but has not been commercialized is the use of a magnetorheological (MR) damper as the shock absorber damping element [10, 11, 12]. The main advantage of MR dampers is that the damping coefficient can be actively controlled by controlling the intensity of the magnetic field applied to the MR fluid. Due to its inherent nonlinear and hysteretic characteristics, several models have been proposed to represent the MR fluid's stress-strain behavior as the intensity of the magnetic field is varied [13, 14].

One characteristic of all three of the semi-active mountain bike suspension designs discussed above is that they utilize a simple on-off control algorithm to control the state of the damper. To switch between the damper soft and stiff setting, these three designs use an acceleration threshold value. If the acceleration is above the threshold value the damper setting will become soft, once the acceleration drops below the threshold value the damper setting will become stiff again.

### 2.1.3 Ride Characteristics of Full Suspension Bicycles

While full suspension bikes offer some advantages, as described above, it has been suggested that they are less efficient than bikes with only a front suspension due to increased energy lost to damping in the rear shock and the dissipation of energy generated through "bobbing". Bobbing is a cyclic, up-and-down motion of the bike frame caused by the pedaling motion of the rider [15]. Several studies in the literature have examined the effect of bobbing on riding efficiency, with varying results [3, 16, 17]. While full suspension bikes may be less

efficient at transforming energy at the pedals into potential and kinetic energy of the bike, a substantial enhancement of rider comfort and control appears to offset these losses in mechanical efficiency so that the overall efficiency of the rider/bicycle system is not appreciably different between a full suspension design and a design with front suspension only.

## 2.2 Existing Studies on Vibration Analysis of a Bicycle

This section describes studies in which vibrations generated in a bicycle during use are analyzed. Experimental methods and results of these studies are discussed.

### 2.2.1 In-house and Field Set-up and Testing

To test and analyze vibrations of a bicycle, experimental set-ups have been designed to reproduce a good road surface in a lab using actuators to input vibrations to the rear wheel of a bicycle [6, 7]. Many methods have been used to stabilize and balance a bicycle in the upright position so that the bicycle would not fall during the tests. Amongst these methods are the use of bungee cords strapped to different locations on the bicycle. To represent the cyclist sitting on the bicycle, weights were attached to the saddle and each handle; where most of the weight was located at the saddle. Assessment tests were done using different types of bicycles with accelerometers mounted at the dropouts, seat clamp and under the saddle. The tests were performed on smooth and coarse surfaces to continuously excite the bicycle, and over traffic bumps to produce single load inputs. The data was collected using an acquisition module and laptop that were wired to the accelerometers. The data acquisition module and laptop were placed in a backpack worn by the rider for the road tests. The data of these experiments were then plotted on transmissibility, acceleration response, and power spectral density (PSD) plots to determine the structural response of the bicycle as it is excited through vibrations at the rear wheel.

### 2.2.2 Effects of Adding a Rider to the Bicycle Structure Dynamics

Some research has been conducted to determine if adding a rider to a bicycle system would cause any change in the structural dynamics of a bicycle. One of the methods used to further understand the dynamic behavior of a bicycle structure was by performing experimental modal analysis (EMA) [4]. Vibration modes of a bicycle structure were determined using different operating conditions with and without a cyclist while testing the system on test rigs in a laboratory and roadways. Accelerometers mounted to different locations throughout the bike would be used to measure the structural response as the bicycle is excited through vibrations at the front and rear wheels. The tests conducted in a previous study shows that the mode shapes of the bicycle structure change frequencies when a rider is introduced to the bicycle [4]. This shift indicates that introducing a rider to the system has a strong influence on the dynamics of a bike.

## 2.3 Use of MR Fluids in Mechanical Dampers

This section discusses the three types of settings MR fluids can be used: shear mode - in which fluid flows between two parallel surfaces, flow mode or valve mode - in which fluid flows through an orifice, and squeeze mode - in which the fluid is put into compression between two parallel plates [2]. Each of the following subsection elaborates on one of the three settings.

### 2.3.1 Flow Mode (Valve Mode)

Flow or valve mode is the most widely used mode of MR fluids. In the flow mode, the MR fluid flows between stationary plates where the viscosity of the fluid varies by applying a magnetic field. The region where the viscosity of the fluid is being altered is where the MR fluid is exposed and passes through the magnetic flux lines. Common devices that operate in this mode include servo valves, dampers, shock absorbers and actuators. For further detail on how

MR fluids are used in the flow mode of dampers please refer to the Introduction and Methods chapters.

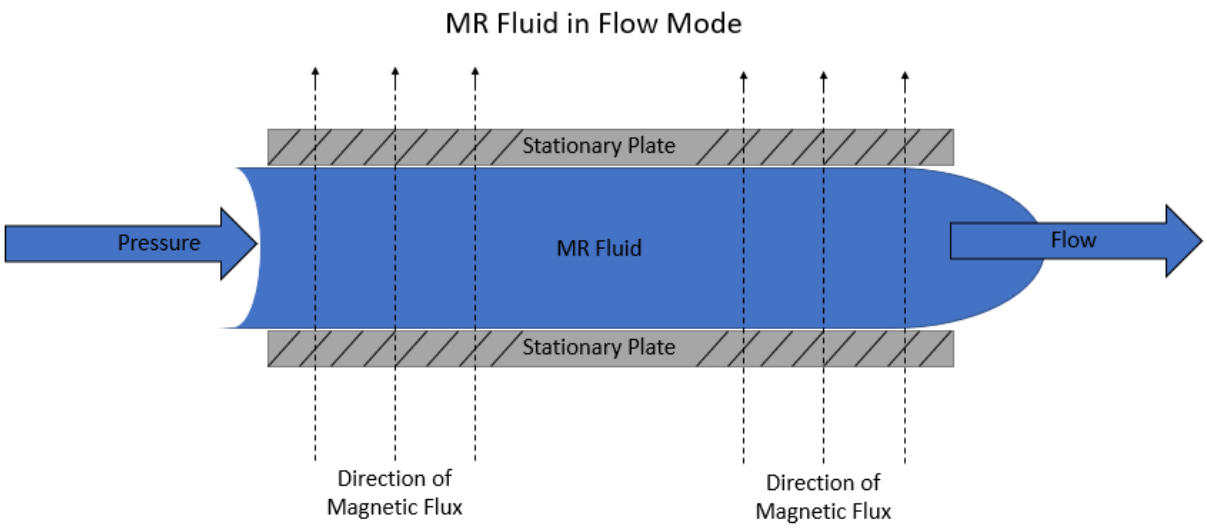


*Figure 2.1 - Flow Mode*

### 2.3.2 Shear Mode

The second use of MR fluid is in the shear mode. In this mode, MR fluid is suspended between either a stationary surface and a movable surface (which moves parallel to the stationary surface) or two movable surfaces; where the magnetic field acts perpendicular to the direction of motion of the movable surface(s). Some examples of devices in shear mode are brakes, clutches, dampers, locking devices and structural composites.

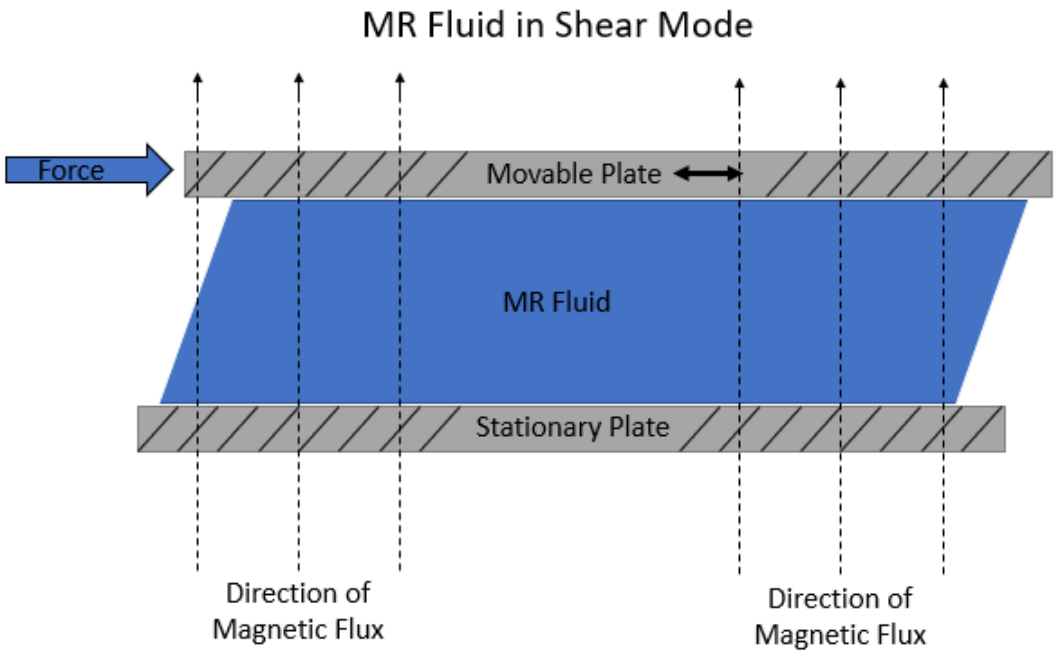


*Figure 2.2 - Shear Mode*

### 2.3.3 Squeeze Mode

The third use of MR fluid is in the squeeze mode, which operates similar to the shear mode. The MR fluid is suspended between either a stationary surface and a movable surface or two movable surfaces, such that the movable surface(s) move(s) perpendicular to the stationary surface(s) (the distance between the two surfaces becomes larger or smaller depending on the direction of motion). Relatively high forces can be achieved using this type of mode. The best use of this mode would be for vibration dampers which experience low amplitudes and high dynamic forces. These dampers operate by having a disc move through a chamber of MR fluid such that the motion is initially axial and then transitions to lateral motion. The induction of a magnetic field causes the MR fluid to transition from a viscous to a viscoelastic state (exhibiting both elastic and viscous behavior when deformed).

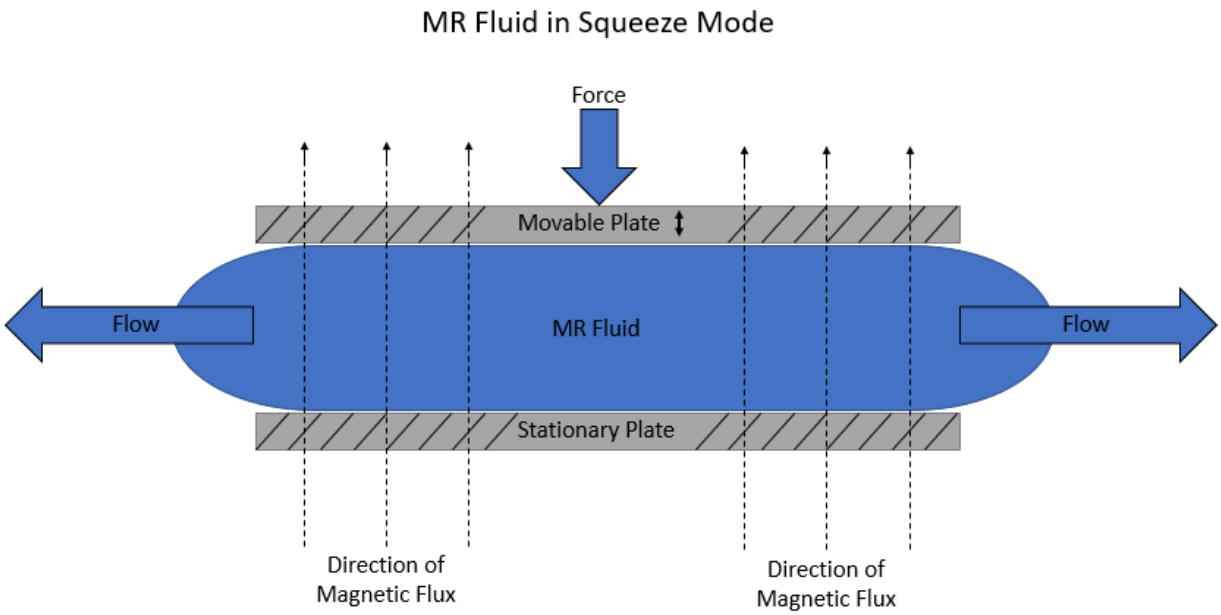


*Figure 2.3 - Squeeze Mode*

## 2.4 Studies using Bicycles with MR Dampers

The development of semi-active damping suspensions on mountain bikes in the 2000's led to the use of a magnetorheological (MR) damper as the shock absorber damping element. Studies were done to see how implementing the MR damper as the shock absorber damping element would affect the accelerations at the saddle [10, 11, 12]. One of these studies used MR dampers in the front and rear suspension while the others only implemented the MR damper in the rear shock system. Each study used accelerometers mounted at the rear axle and saddle. The tests were done using a sinewave sweep at 1, 2, 3, and 4 Hz and on a smooth road surface with a slight incline and an off-road downhill trail. For each testing condition the current supplied to the damper was set to 0.0 A, making the shock act as a passive damper, and at a second current that saturates the MR damper, such that it has the highest possible damping coefficient.

The goal of these studies was to achieve an automatic transition between high pedal efficiency on smooth terrain and comfort with trail contact on rough terrain using semi-active

damping. The results from the variety of tests performed give some evidence that semi-active MR dampers may be used to effectively transition between the high pedal efficiency and comfort with trail contact. Tests done on smooth trails and with the current input set at 0.0 A, have large frequency responses due to pedal bob motions (unwanted oscillations due to pedaling) which were expected. When the same trail was tested using a current input that saturated the MR damper, the frequency response was significantly suppressed and approached the ideal behavior. Tests done on an off-road trail had the reverse effects. When the current input was set at 0.0 A, the frequency response had a much larger reduction in vibration at the saddle as compared to the saturated MR damper. It should be noted that all testing has been done using an on/off control algorithm only.

# CHAPTER THREE: METHODS

This chapter presents the experimental set up and control strategy used to test the magnetorheological damper-based shock absorber. The overall design of the rear shock absorber that was developed during this study has been included in this chapter. This chapter also presents a mathematical model that can be used for preliminary analysis to understand the dynamics of the bike.

## 3.1 MR Damper-Based Shock Absorber - Design

Dual suspension mountain bikes are designed to find the balance between shock absorption (on rough trails) and high pedaling efficiency (on smooth trails). The 2014 Specialized Epic "cross-country" mountain bike is such a bike; it incorporates a hydraulic inertia valve system to strike this balance. For this research, the hydraulic inertia valve system was removed and replaced with the MR damper-based shock absorber. To install the new shock, which is shown in Figure [3.1], custom links were fabricated from aluminum such that they fit into the existing suspension linkage without altering the kinematics of the linkage. The MR damper-based shock absorber was constructed using a commercially available MR damper (Manufacturer: Lord Corporation, Model: RD 8040-1) and a pair of air springs (Manufacturer: Bimba, Model: SR-042-DPY). The air springs were mounted symmetrically about the frame such that one was positioned on either side of the damper. Each of these air springs contain separate compression and rebound chambers that can be pressurized independently from each other. There were three geometric constraints accounted for when designing the MR damper-based shock absorber: the existing frame and suspension linkage mounting locations (constraining the length of the shock) and the legs of the rider (constraining the width of the

shock). Since the MR damper-based shock absorber was intended for experimental use, the design did not minimize volume or weight.

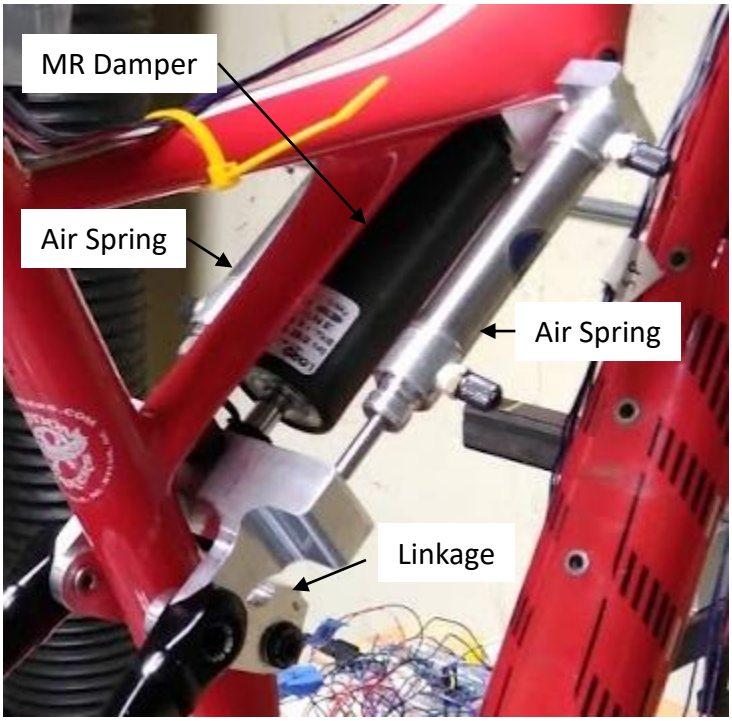


*Figure 3**Error! Use the Home tab to apply 0 to the text that you want to appear here.**.4 The MR damper-based rear mountain bike shock absorber*

A schematic diagram of the MR damper-based shock absorber system is shown in Figure [3.2], and a picture of the full experiment is shown in Figure [3.3]. The MR damper is a piston-based damper with a coaxial electromagnetic coil located near the piston orifices. A variable current between 0 and 1.5 Amperes can be passed through the coil using a current amplifier (Manufacturer: Lord, Model: Wonder Box®). When the current is passed through the coil, a magnetic field is created in the piston orifices, increasing the viscosity of the MR fluid and subsequently increasing the damping coefficient. This current delivered to the damper coil is controlled by a 32 bit, Atmel SAM8XE microcontroller running at 84 Mhz. and mounted on an Arduino Due development board. An unsigned (positive) integer, referred to as the "shock number," is assigned by the microcontroller to set the MR coil current. The value of this shock

number is written to a D to A converter (DAC) which converts the number to an analog control voltage between 0 and 5 Volts. This voltage is used as a control signal to the current amplifier, which puts out a current that is proportional to the control voltage. Three different 3-axis MEMS accelerometers are mounted to the bike, one near the rear axle, one on the seat post, and one near the handlebars and act as inputs to the microcontroller. These accelerometers can be used strictly for data acquisition, when the system is run with a constant damper current, or for data acquisition and as control inputs, when the system is running in feedback control mode.

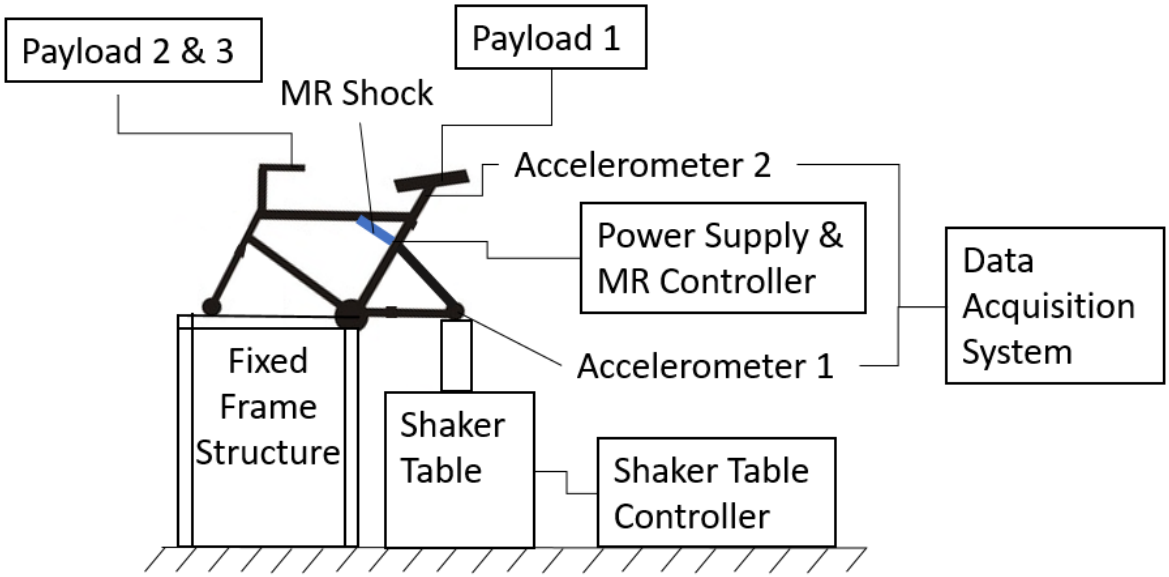


*Figure 3.5 Schematic diagram of the shaker-table experiment*

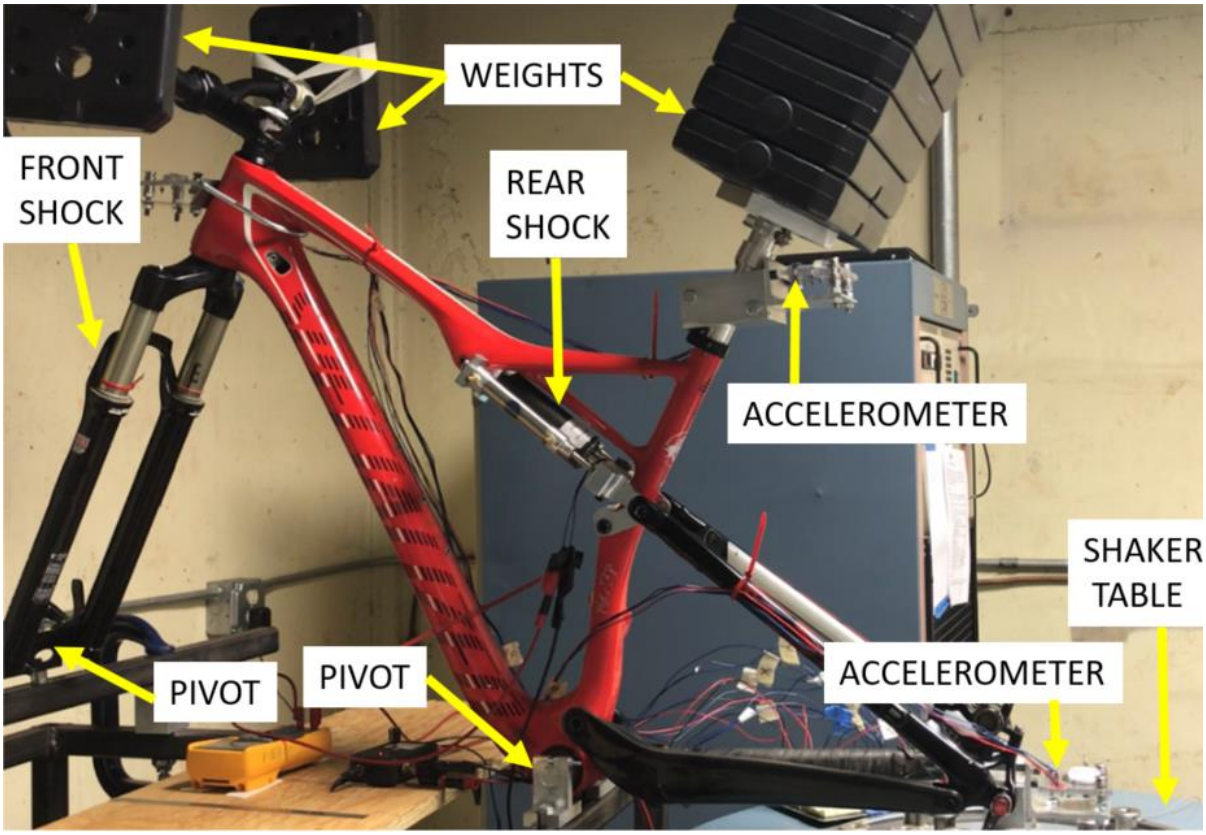


*Figure 3.6 The shaker-table experimental set up*

### 3.2 Shaker Table Testing

To investigate the bike response to the MR damper-based shock absorber, the original shock absorber plus inertia valve was removed and replaced with the MR shock absorber system, as shown in Figure [3.1]. The MR shock absorber was assembled to the bike using the new linkage design described in the previous section. The bike's rear axle was attached to the actuator platform of a single degree-of-freedom shaker table (Manufacturer: Unholtz Dickie, Model: S452 LP) after removing the rear wheel. To orient the frame such that the vertical motion of the actuator platform remains perpendicular to the bottom links of the rear triangle, a fixture was fabricated from steel tubing to support the front end of the bike. The crank arm and pedals were removed from the bike to allow the bike to be mounted to the fixture using the bottom bracket bearings of the bike. This allowed the frame to rotate about the bottom bracket but not translate,

as can be seen from Figure [3.3]. The front wheel was removed, allowing the front fork of the bike to also mount to the fixture using the front axle mount. This allowed the linear joint of the front fork to move, while the wheel mounting point was only allowed to rotate.

The interaction of forces between a mountain bike rider and the bike is complex and difficult to simulate in a laboratory setting. In the shaker table test set up, external forces have been applied to the bike at the rear axle by the shaker, at the powertrain axis by the fixture mount, at the front axle by the fixture mount, and by weights mounted at the seat post and on the handlebars. The seat post weights had a mass of 39.7 kg, and each handlebar weight had a mass of 3.2 kg. The distribution of mass of a typical rider at different locations of the bike was found from the literature [18].

The air spring in the front fork of the bike was pressurized to 480 kPa, which is listed by the manufacturer as the appropriate pressure for a rider with the mass described above. Pressure in the air springs of the MR shock absorber assembly was set using a common approach used to set up a mountain bike suspension for a particular rider. This approach involves watching the compression of the suspension as the weights are applied and using a pressure that displaces the shock at the middle of its stroke. This resulted in a pressure of 550 kPa in both the compression and rebound sides of the cylinders.

### 3.3 Suspension Control and Data Acquisition

Data acquisition and control of the damper current was accomplished through the Atmel SAM8X microcontroller. The accelerations at the rear axle and at the seat post of the bike were measured using three-axis MEMS accelerometers. Acceleration data was recorded onto a microSD card using a serial-peripheral-interface (SPI) bus at a sampling rate of 5 milliseconds using the 10-bit A to D converters on the microcontroller. The microcontroller code generates an

integer proportional to the desired coil current, which the D to A converter (DAC) converts to a DC voltage which is used as the control signal to the current amplifier to deliver the desired coil current through the MR damper.

The response of the MR shock absorber was measured on the shaker table by using a series of constant, sinusoidal inputs and by using a sine sweep input. The set frequencies were 2, 5, 10, and 20 Hz while the sine sweep of 1 - 20 Hz over 20 seconds was used. Each input condition was run at damper currents of 0.0 A, 0.4 A, and 1.4 A. The 0.0 A current results in the softest setting of the damper while the 1.4 A current results in magnetic saturation (the stiffest damper setting). By experimenting with the system, it was found that a current of 0.4 A resulted in damping that was near the mid-point between the 0.0 A damping and the 1.4 A damping.

### 3.4 Trail Testing

Since the interactions between the trail, bike, and rider are complex and difficult to reproduce in a laboratory setting, testing was also conducted on a mountain trail to test the effects of different damper control settings on trail response. The bike was removed from the shaker table and the wheels, saddle, and drive components were re-assembled to the bike. The accelerometer mount located near the saddle was redesigned such that it mounts directly under the saddle to best capture the acceleration felt by the rider. The accelerometer mount at the rear axle also had to be redesigned such that it mounts to the side of the rear triangle as close to the rear axle as possible to best capture the acceleration input at the rear wheel. The wires for each of the accelerometers and the MR damper were then routed to a backpack that held the microcontroller board and peripherals, the current amplifier, and a 2 Ah, 24 VDC battery (Manufacturer: Kobalt, Model: KB 224-03) that was used to power the controls and to supply current to the MR damper. The backpack was worn by an experienced mountain biker with a

mass of 86 kg during testing, as shown in Figure [3.4]. The pressure in the front shock air spring was set to the manufacturer's recommendation of 820 kPa, while the pressure in the rear air springs was set to 890 kPa in both the compression and rebound chambers.

*Figure 3.7 - MR Shock-Equipped Bike on Trail*

A rocky trail with a moderate downhill slope and a surface of hard-packed dirt with gravel and rocks was used to test the control algorithm while measuring accelerations. The data was collected using three different damper currents set at 0.0 A, 0.4 A, and 1.4 A. An on-off control algorithm and a proportional control algorithm was also used during the trail tests. The on-off control algorithm is governed by the following logic:

$$if\ \ ((a_n + a_{n-1}) > t_{uo}\ \ or\ \ (a_n + a_{n-1}) < t_{lo}$$

$$then\ \ s = s_{soft}$$

$$else\ \ s = \ s_{stiff} \tag{3.1}$$

Where $a_n$ is the n[th] data point of the rear-axle accelerometer z-component and $a_{n-1}$ is the (n-1)[th] data point of the rear-axle accelerometer z-component, $t_{uo}$ is the upper threshold for the sum of two acceleration readings for the on/off controller, $t_{lo}$ is the lower threshold for the sum of two acceleration readings for the on/off controller, $s$ is the shock number that sets the current in the MR damper, $s_{soft}$ is the shock number corresponding to no current, and $s_{stiff}$ is the shock number corresponding to saturation current.

To reduce the possibility that the controller will react to noise, the control algorithm uses the sum of two consecutive acceleration measurements. Since these acceleration values can be positive or negative the absolute value of this sum is used. The threshold values for the on-off controller were set to correspond to an acceleration of $\pm$8.1 m/s2 (approximately 0.8g). When the sum of the two accelerations is below the threshold value, the shock is in its stiffest possible state to improve handling and pedaling efficiency. When the sum of accelerations exceeds the threshold, the shock is switched to its softest possible state, which should result in higher ride comfort.

The control algorithm for proportional control is governed by the following logic:

$$e = \ a_0 - (a_n + \ a_{n-1}) \tag{3.2}$$

$$if\ \left(e > \ t_{up}\ \ or\ \ e < \ t_{lp}\right) \tag{3.3}$$

$$then\ \ s = \ s_{stiff} - m * e$$

$$else\ \ s = \ s_{stiff}$$

where $e$ is the constant of proportionality, $a_0$ is the absolute value of two consecutive accelerometer readings when rear axle acceleration is zero, $t_{up}$ is the upper threshold for the sum of acceleration readings, and $t_{lp}$ is the lower threshold for sum of two acceleration readings for the proportional controller. The goal of the controller is to minimize acceleration at the seat. A threshold value of 3.8 $m/s^2$ is used to reduce the effects of noise. When the acceleration is below the threshold, the shock is set to its stiffest state. When the acceleration exceeds the noise threshold, the current through the MR damper is reduced in proportion to the acceleration to enhance ride comfort.

All acceleration values are initially stored as an array of integers from the microcontroller A to D converters. The arrays are then post-processed in MATLAB® in order to convert them into acceleration values with the appropriate units of $m/s^2$.

### 3.5 Mathematical Model

A mathematical model of a dual suspension mountain bike was developed using the governing equations of motion (EOM). This is an in-plane model and captures the dynamics of the bike while traveling in a straight line. The model is divided into four rigid bodies that are connected through the suspension systems, the seat stay frame link (Link 1), and chain stay frame link (Link 2). Each suspension system and the seat stay frame link and chain stay frame link is represented as a spring damper unit. A diagram of the bike is shown in Figure [3.5] and layout of the model is shown in Figure [3.6]. The diagram of the bike consists of six unique bodies: the frame, front fork, shock system, link 1, link 2, and link 3 (The wheels were not included in the diagram since they were to be removed from the bike for the shaker table testing). All joints between the six bodies are pin joints except for the connection between the frame and

the front fork; which is a sliding joint. The rider weight was distributed between the saddle and the handlebars. The purpose of the mathematical model shown in Figure [3.6] is to be used for preliminary analysis to understand the dynamics of a dual suspension bike. The model was represented in this way (under "normal conditions" of a bike where the bike is free to move in any direction) because it allows for preliminary analysis under "normal conditions" or under any type of constrains (such as the shaker table set-up) by manipulating the mass, stiffness, and damping coefficients.

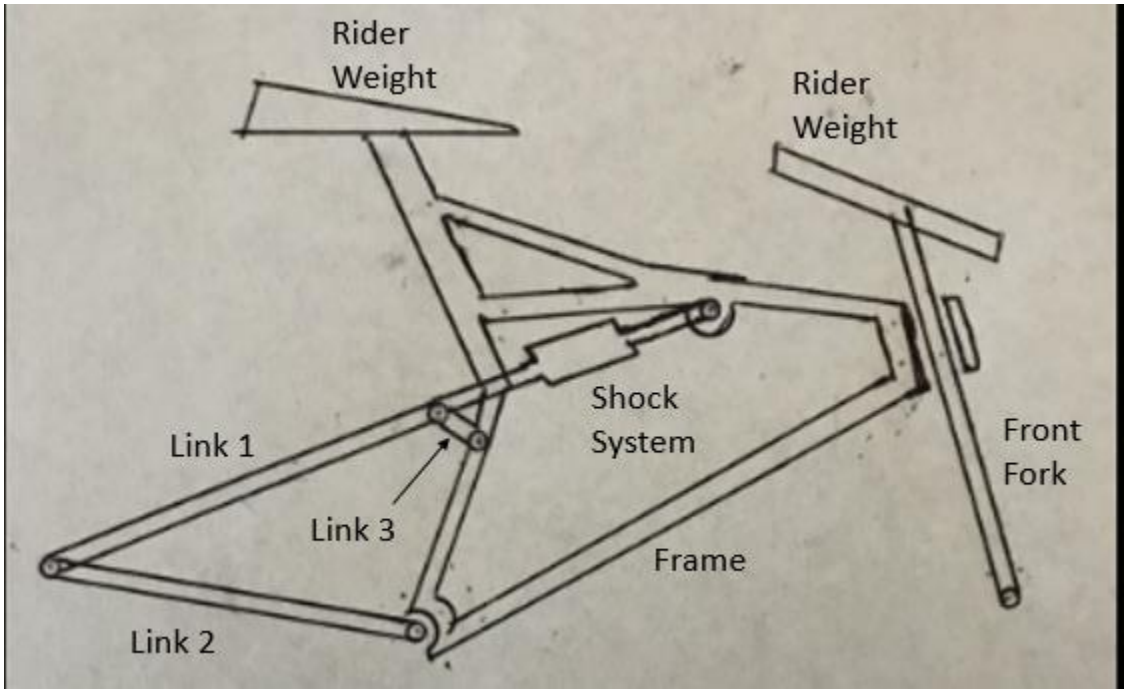


*Figure 3.8 - Dual Suspension Mountain Bike (no wheels are shown)*

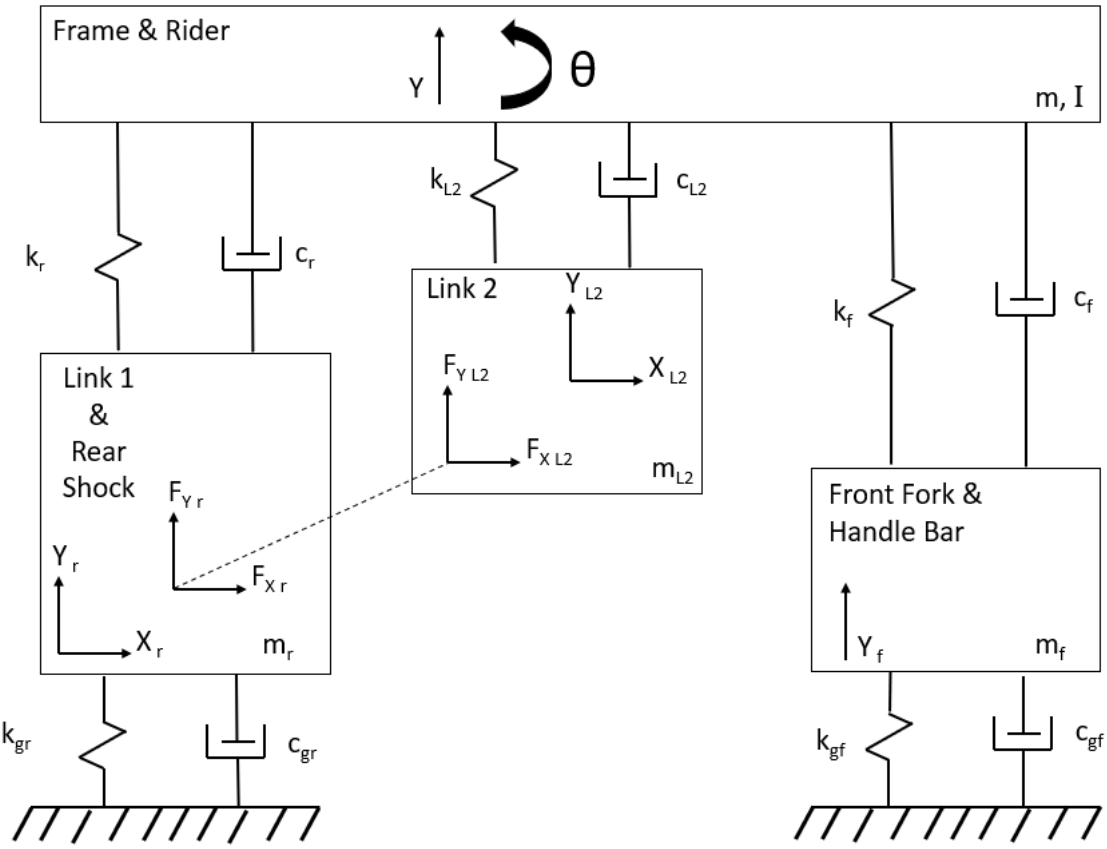


*Figure 3.9 - Full Suspension Mountain Bike Mathematical Model*

The rigid body representing the combined bicycle frame and rider has been modeled with two degrees-of-freedom (DOF), a translation in the vertical (Y) direction and a rotation about an axis perpendicular to the plane of the bike frame (the Z direction, located at the power train axle). This combined mass is referred to as the sprung mass. It may be noted that no distinction has been made between the bicycle frame and the rider, the rider is assumed to be rigidly attached to the frame. The EOM for the sprung mass are derived to be as follows:

$$m\ddot{y} + \left(k_f + k_r + k_{L2}\right)y - k_f y_f - k_r y_r + \left[k_f(p-b) - k_r b\right]\theta + (-k_{L2})y_{L2} + \left(c_f + c_r + c_{L2}\right)\dot{y} - c_f \dot{y}_f - c_r \dot{y}_r + \left[c_f(p-b) - c_r b\right]\dot{\theta} + (-c_{L2})\dot{y}_{L2} = 0 \quad (3.4)$$

$$I\ddot{\theta} + \left[k_f(p-b)^2 + k_r b^2\right]\theta + \left[k_f(p-b) - k_r b\right]y - k_f(p-b)y_f + k_r b y_r + \left[c_f(p-b)^2 + c_r b^2\right]\dot{\theta} + \left[c_f(p-b) - c_r b\right]\dot{y} - c_f(p-b)\dot{y}_f + c_r b\dot{y}_r = 0 \quad (3.5)$$

In Eq. (3.4), $m$ is the sprung mass and in Eq. (3.5), $I$ is the mass moment of inertia of the sprung mass about the z-axis passing through the center of mass as per the coordinate system in Figure [3.6] (the z-axis is directed into the page). The vertical displacement (bounce) of the sprung mass is represented by $y$ and the in-plane (pitch) rotation of the sprung mass is represented by $\theta$. Furthermore, $p$ is the wheelbase (distance between the contact point of the front tire and the contact pint of the rear tire) and $b$ is the distance from the center of mass of the sprung mass to the contact point of the rear tire. In Eqs. (3.4) and (3.5), $k_f$ and $c_f$ are the equivalent stiffness and damping constants of the front suspension, and $k_r$ and $c_r$ are the equivalent stiffness and damping constants of the rear suspension (link 1 and MR damper-based shock absorber). Note that link 3 in Figure [3.5] does not apply stiffness or damping to the system but is instead used to keep link 1 and the MR damper-based shock absorber in line with each other; thus it is not necessary to include link 3 in the model and the stiffness and damping constants of the link 1 and the shock can be added together and act on the system as one body. Also, $y_f$ and $y_r$ are the vertical displacements of the front and rear unsprung mass respectively. It may be noted that each unsprung mass is the combined mass of the wheel and other parts connected to the wheel such as the tire, brake, axle, and related hardware. Note that although the

model includes the hardware and wheels, the shaker table testing had these parts removed and the mass ($m$, $m_f$, and $m_r$), stiffness constants ($k_{gf}$ and $k_{gr}$), and damping constants ($c_{gf}$ and $c_{gr}$) were adjusted to account for wheel removal. Finally, $k_{L2}$ and $c_{L2}$ are the vertical stiffness and damping constants of the chain stay frame link, as seen in Figure [3.6].

The front unsprung mass ($m_f$) has been modeled with only one DOF while the rear unsprung mass ($m_r$) has been modeled with two DOF. This is because the rear unsprung mass is attached to the frame through the chain stay frame link, connected through a pin joint on the frame and a pin joint at the rear axle, as shown in the schematic of the model in Figure [3.6]. The front unsprung mass is only connected to the front suspension. The EOM for the front unsprung mass and the rear unsprung mass are derived as:

$$m_f\ddot{y}_f - k_f y - k_f(p-b)\theta + \left(k_f + k_{gf}\right)y_f - c_f\dot{y} - c_f(p-b)\dot{\theta} + \left(c_f + c_{gf}\right)\dot{y}_f = 0 \tag{3.6}$$

$$m_r\ddot{x}_r = F_{xr} \tag{3.7}$$

$$m_r\ddot{y}_r + \left(k_{gr} + k_r\right)y_r - k_r y + k_r b\theta + \left(c_{gr} + c_r\right)\dot{y}_r - c_r\dot{y} + c_r b\dot{\theta} = F_{yr} \tag{3.8}$$

In Eqs. (3.6), (3.7) and (3.8), $y_r$ and $x_r$ are the vertical and fore-aft displacements of the rear unsprung mass while $y_f$ is the vertical displacement of the front unsprung mass. Also, $k_{gf}$ and $c_{gf}$ are the equivalent stiffness and damping constants of the front tire, and $k_{gr}$ and $c_{gr}$ are the equivalent stiffness and damping constants of the rear tire (again note that these stiffness and damping constants are manipulated to represent the shaker table testing which does not include the wheels and some hardware). $F_{xr}$ and $F_{yr}$ are the interaction forces between the rear unsprung mass and the chain stay frame link, resulting from the chain stay frame link connection at the

rear axle. This mathematical model has been adapted from an in-plane model of a motorcycle. Although there are many differences between the layout of a motorcycle and a mountain bike, there are specific similarities due to the presence of the rear suspension system [19].

The chain stay frame link unsprung mass ($m_{L2}$) has been modeled with two DOF. The EOM for the chain stay frame link unsprung mass are derived as:

$$m_{L2}\ddot{x}_{L2} = F_{x\,L2} \tag{3.9}$$

$$m_{L2}\ddot{y}_{L2} + (k_{L2})y_{L2} + (-k_{L2})y + k_{L2}b\theta + (c_{L2})\dot{y}_{L2} + (-c_{L2})\dot{y} + c_{L2}b\dot{\theta} = F_{y\,L2} \tag{3.10}$$

In Eqs. (3.9) and (3.10), $y_{L2}$ and $x_{L2}$ are the vertical and fore-aft displacements of the chain stay frame link unsprung mass. Also, $k_{L2}$ and $c_{L2}$ are the stiffness and damping constants of the chain stay frame link. Furthermore, $F_{x\,L2}$ and $F_{y\,L2}$ are the interaction forces at the chain stay frame link due to the connection between the frame and the rear axle.

The mathematical model and EOM described above were designed for a dual suspension mountain bike. The mass ($m$, $m_f$, and $m_r$), stiffness constants ($k_{gf}$ and $k_{gr}$), and damping constants ($c_{gf}$ and $c_{gr}$) were manipulated such that the model would represent a 2014 Specialized mountain bike attached to a shaker table, described in section (3.2).

The EOM from Eqs. (3.4) through (3.10) can be combined in order to form the mass ($M$), damping ($C$), and stiffness ($K$) matrices of the system, all three of which are $7 \times 7$.

$$M = \begin{bmatrix} m,0,0,0,0,0,0 \\ 0,I,0,0,0,0,0 \\ 0,0,m_f,0,0,0,0 \\ 0,0,0,m_r,0,0,0 \\ 0,0,0,0,m_r,0,0 \\ 0,0,0,0,0,m_{L2},0 \\ 0,0,0,0,0,0,m_{L2} \end{bmatrix} \tag{3.11}$$

$$C = \begin{bmatrix} c_{fy}+c_{ry}+c_{L2y}, -(b-p)*c_{fy}-p*\left(c_{L2y}+c_{ry}\right), -c_{fy},0,-c_{ry},0,-c_{L2y} \\ -(b-p)*c_{fy}-p*\left(c_{L2y}+c_{ry}\right), (b-p)^2*c_{fy}+p^2*\left(c_{L2y}+c_{ry}\right), -(b-p)*c_{fy},0,-p*c_{ry},0,-p*c_{L2y} \\ -c_{fy}, -(b-p)*c_{fy}, c_{gf}+c_{fy},0,0,0,0 \\ 0,0,0,c_{rx}+c_{L2x},0,-c_{rx},0 \\ -c_{ry}, -p*c_{ry},0,0,c_{ry}+c_{L2y},0,-c_{ry} \\ 0,0,0,-c_{rx},0,c_{L2x}+c_{rx},0 \\ -c_{L2y}, -p*c_{L2y},0,0,-c_{ry},0,c_{ry}+c_{L2y} \end{bmatrix} \tag{3.12}$$

$$K = \begin{bmatrix} k_{fy}+k_{ry}+k_{L2y}, -(b-p)*k_{fy}-p*\left(k_{L2y}+k_{ry}\right), -k_{fy},0,-k_{ry},0,-k_{L2y} \\ -(b-p)*k_{fy}-p*\left(k_{L2y}+k_{ry}\right), (b-p)^2*k_{fy}+p^2*\left(k_{L2y}+k_{ry}\right), -(b-p)*k_{fy},0,-p*k_{ry},0,-p*k_{L2y} \\ -k_{fy}, -(b-p)*k_{fy}, k_{gf}+k_{fy},0,0,0,0 \\ 0,0,0,k_{rx}+k_{L2x},0,-k_{rx},0 \\ -k_{ry}, -p*k_{ry},0,0,k_{ry}+k_{L2y},0,-k_{ry} \\ 0,0,0,-k_{rx},0,k_{L2x}+k_{rx},0 \\ -k_{L2y}, -p*k_{L2y},0,0,-k_{ry},0,k_{ry}+k_{L2y} \end{bmatrix} \tag{3.13}$$

Using a base excitation corresponding to the shaker table displacement at the rear axle, displacement transmissibility is computed from the EOM. Displacement transmissibility is the ratio of the maximum displacement with the input displacement. For the model developed in this study, displacement transmissibility due to external excitation is derived as:

$$T = \left[-\omega^2 M + i\omega C + K\right]^{-1}\left[\acute{K} + i\omega\acute{C}\right] \tag{3.14}$$

In Eq. (3.14), $T$ is the 7 × 1 transmissibility matrix, and $\omega$ is the excitation frequency, while $\acute{K}$ and $\acute{C}$ are 7 × 1 matrices resulting from the source of base excitation.

$$\acute{K} = [0,0,0,0,k_{gr},0,0] \tag{3.15}$$

$$\acute{C} = [0, 0, 0, 0, c_{gr}, 0, 0] \tag{3.16}$$

In order to solve for the system response in time domain, the EOM from Eqs. (3.4) to (3.10) are compiled in a state space model that is expressed as follows:

$$\begin{bmatrix} \dot{X}_1 \\ \dot{X}_2 \end{bmatrix} = \begin{bmatrix} Z_{7,7} & I_{7,7} \\ -M^{-1}K & -M^{-1}C \end{bmatrix} \begin{bmatrix} X_1 \\ X_2 \end{bmatrix} + \begin{bmatrix} Z_{7,1} \\ M^{-1}F \end{bmatrix} \tag{3.17}$$

In Eq. (3.17), $X_1 = \begin{bmatrix} y & \theta & y_f & x_r & y_r & x_{L2} & y_{L2} \end{bmatrix}^T$ is a 7 × 1 matrix and $\dot{X}_1 = X_2$. $Z_{7,7}$ and $Z_{7,1}$ are 7 × 7 and 7 × 1 zero matrices respectively, while $I_{7,7}$ is a 7 × 7 identity matrix. Also, *F* is the time varying force matrix that consists of input force that serves as external excitation to the system that is transmitted through the rear axle.

In order to evaluate transmission of vibration to the seat, the frequency response function (FRF) for accelerations of all DOF resulting from excitation at the rear axle is computed from the EOM listed in Eqs. (3.4) through (3.10), the FRF matrix for the system, $H(\omega)$, is expressed as:

$$H(\omega) = -\omega^2[-\omega^2 M + i\omega C + K]^{-1}\left[\hat{K} + i\omega\hat{C}\right] \tag{3.18}$$

In Eq. (3.18), $\hat{K}$ and $\hat{C}$ are 7 × 1 matrices resulting from the source of base excitation as follows:

$$\hat{K} = [0, 0, 0, 0, k_{gr}, 0, 0]^{-1} \tag{3.19}$$

$$\hat{C} = [0, 0, 0, 0, c_{gr}, 0, 0]^{-1} \tag{3.20}$$

$H(\omega)$ is also 7 × 1 and computes the accelerations of all DOF due to excitation at the rear axle.

In order to account for a random road profile, power spectral density (PSD) has been used to evaluate ride comfort and handling from acceleration levels. A PSD is the measure of signal's power content versus frequency and is used to quantify random vibration fatigue. In other words, PSDs represent the energy in the system and will show which frequencies will have stronger (higher or larger) vibration influence and which frequencies will have weaker (lower or smaller) vibration influence on the system. The PSD data from a good road surface was used with the bicycle traveling at a constant velocity of 4.5 m/s (about 10 mph). The "good" road surface is defined as being a smooth paved road with no cracks, bumps, turns, or elevation change. The acceleration PSD for each DOF can be computed as follows:

$$S_{ii}(\omega, V) = |H_i^*(\omega, V)|^2 S_{rr}(\omega, V) \tag{3.21}$$

In Eq. (3.21), $S_{rr}(\omega, V)$ is the PSD of the road profile and $S_{ii}(\omega, V)$ is the PSD of acceleration of each DOF (where, $i = y \quad \theta \quad y_f \quad x_r \quad y_r \quad x_{L2} \quad y_{L2}$) that is computed by using the magnitude of the modified FRF, $H^*(\omega, V)$, corresponding to each DOF. The PSD of the road profile has been computed by assuming a constant speed of the bicycle on a good road surface.

# CHAPTER FOUR: EXPERIMENTAL RESULTS

This chapter presents the results from shaker table testing as well as trail testing at different settings of the MR damper. Some results from the implementation of the control algorithms are also presented. This chapter also presents the results of the mathematical model representation of the shaker table using MATLAB.

## 4.1 Shaker Table Analysis

The shaker table data was collected using three damper currents of 0.0 A, 0.4 A, and 1.4 A with input excitation frequencies of 2, 5, 10, and 20 Hz as well as a sine sweep of 1 - 20 Hz. The data collected from these test conditions were analyzed using MATLAB. After processing the data, two types of plots were used to analyze and understand what is happening between the rear axle and seat post accelerations. RMS (root mean square) plots were used to capture effective acceleration values, while frequency response plots where used to characterize the dynamics of the system. The RMS value of the acceleration can be calculated using the following equation:

$$a_{RMS} = \sqrt{\frac{1}{N}\sum_{n=1}^{N}|a_n|^2} \tag{4.1}$$

Where $N$ is the number of accelerations terms being looked at and $a_n$ is the $n^{th}$ acceleration term.

The RMS acceleration at the rear axle and at the seat post from the shaker table testing is shown in Figure [4.1]. Acceleration values are shown for damper currents of 0.0 A, 0.4 A, and 1.4 A with input excitation frequencies of 2, 5, 10, and 20 Hz. At the 2 Hz input frequency, the effect of stiffening the damper by increasing the damper current can be clearly observed in Figure [4.1 (a)]. As the current is increased from the softest (0.0 A) setting to the mid-range

current (0.4 A) setting to the stiffest (1.4 A) setting, the acceleration at the seat post keeps increasing. The frequency response plots at 2 Hz shows that increasing the damper stiffness increases the relative magnitude of the response at the seat post but the frequencies that are excited do not change.

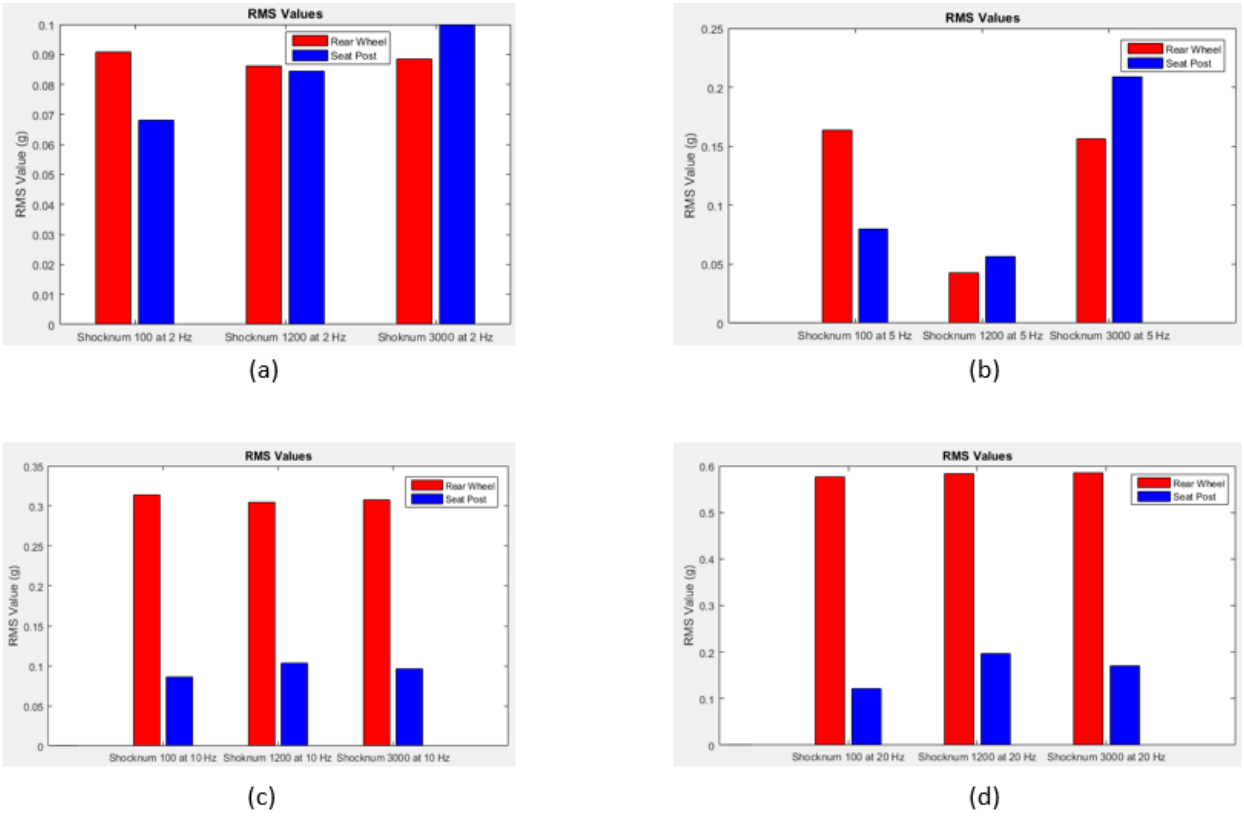


*Figure 4.1 - RMS accelerations measured on the shaker table using damper currents of 0.0, 0.4, and 1.4 A. Measurements at driving frequencies of (a) 2 Hz, (b) 5 Hz, (c) 10 Hz, (d) 20 Hz.*

At 5 Hz, the response of the system to increasing damper current is very different from the response at 2 Hz. As the shock absorber becomes stiffer, the acceleration at the seat post drops initially and then increases significantly, shown in Figure [4.1 (b)]. The frequency response in Figure [4.2], shows that as the current is increased and the damper becomes stiffer, there is a resonance at 5 Hz and the relative magnitude of the seat post response is higher as compared to the input at the rear axle. This resonance at 5 Hz can also be seen in Figure [4.3],

which shows the frequency domain results for a sine sweep input of 1 – 20 Hz at the rear axle. As the damper current is increased, the relative magnitude of the response at the seat post is seen to increase in Figure [4.3], particularly near the 5 Hz resonance. This could be attributed to the frame assembly and the structure holding the seat post on the bike.

At the higher input frequencies of 10 Hz and 20 Hz, observed in Figure [4.1 (c) and (d)], changes in the damper stiffness do not appear to have much effect on the response of the bike at the seat post. As can be seen from Figure [4.3], the damper is still successful in providing isolation at the seat post, however the response does not change significantly with the increase in the damper current.

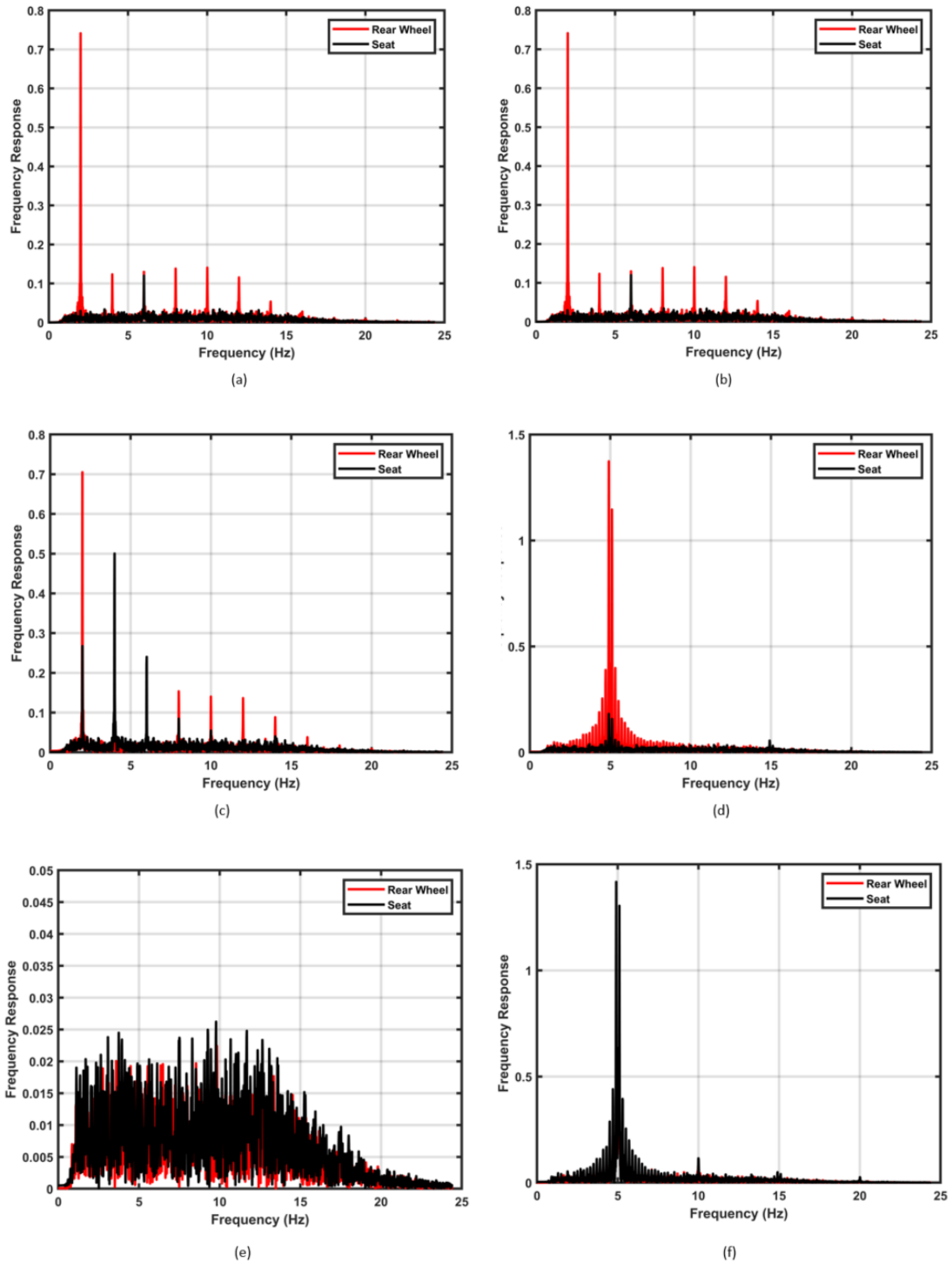


*Figure 4.2 - Frequency response of acceleration at excitation frequencies of 2 Hz and 5 Hz. (a) Frequency = 2 Hz, Current = 0.0 A, (b) Frequency = 2 Hz, Current = 0.4 A, (c) Frequency = 2 Hz, Current = 1.4 A, (d) Frequency = 5 Hz, Current = 0.0 A, (e) Frequency = 5 Hz, Current = 0.4 A, (f) Frequency = 5 Hz, Current = 1.4 A.*

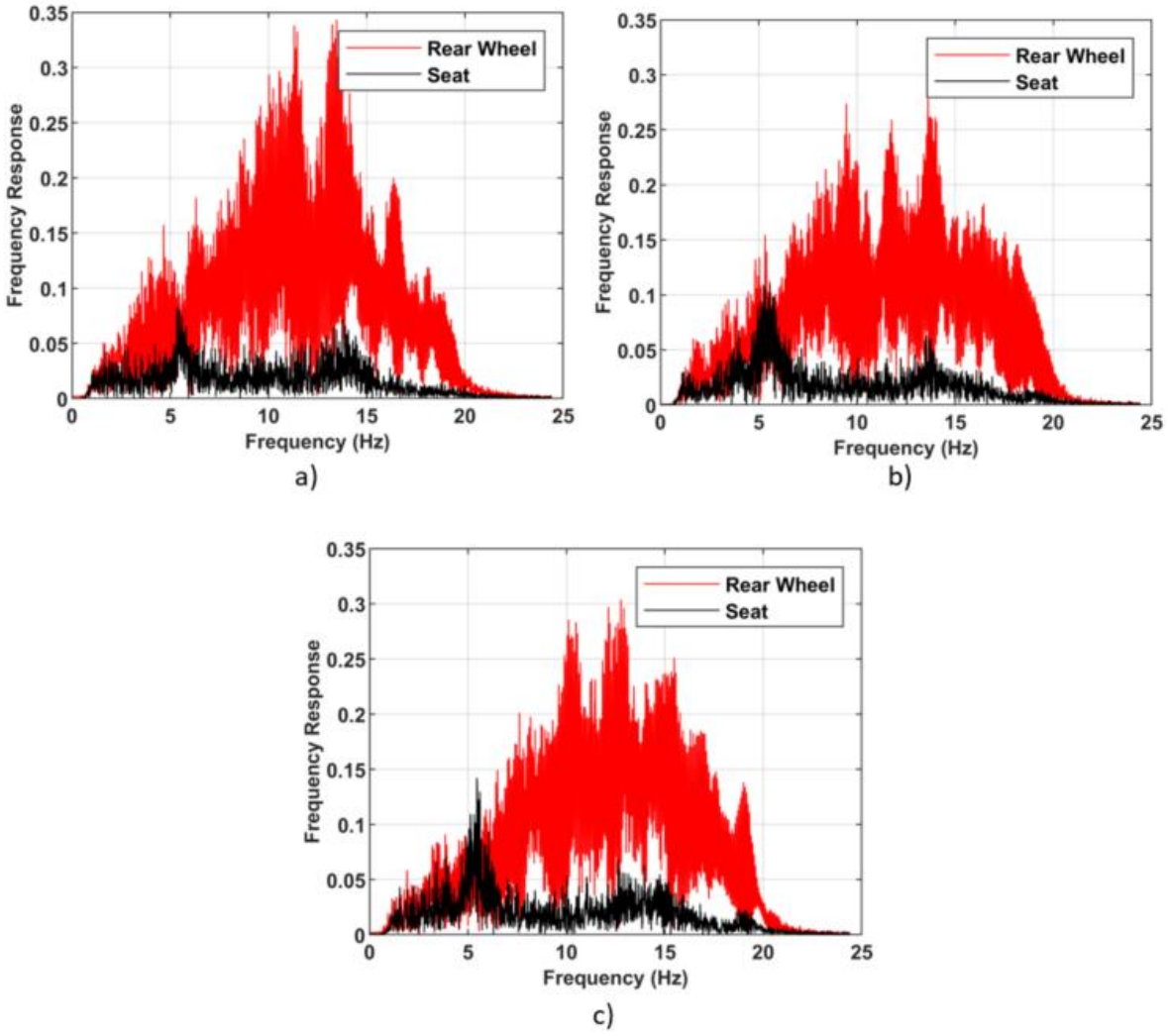


*Figure 4.3 - Frequency response – accelerations measured from sine sweep of 1-20 Hz. (a) Current = 0.0 A, (b) Current = 0.4 A, (c) Current = 1.4 A.*

## 4.2 Trail Testing

The trail data was collected using three damper currents of 0.0 A, 0.4 A, and 1.4 A and two control algorithms - on/off and proportional control, with input excitation at the front and rear wheel due to the rocky trail with a moderate downhill slope and a surface of hard-packed dirt with gravel and rocks. MATLAB was used to process the data and plot the results using RMS and power spectral density (PSD) plots. PSD is used to evaluate the influence of a random road profile.

Figure [4.4] shows the RMS accelerations at the rear axle and the seat post for the three different damper currents and for the two control algorithms – on/off and proportional control. While there is some variation in the data with the changing current, there is no clear effect of changing the damping current on the acceleration at the seat post. However, both control algorithms demonstrate a significant reduction in the acceleration at the seat post, as seen from Figure [4.4].

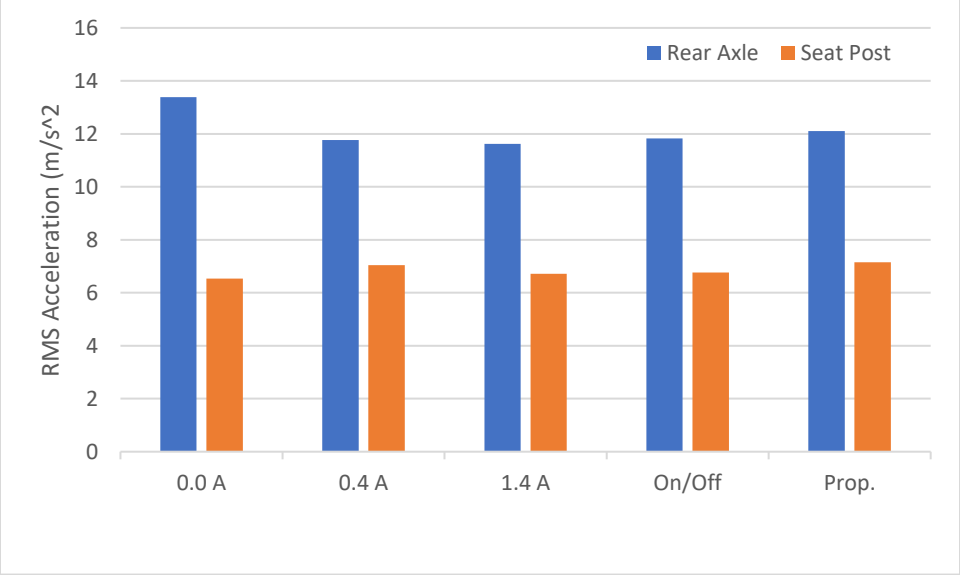


*Figure 4.4 - RMS accelerations – measured on the trail at three different damper currents, with the on/off control algorithm, and with the proportional control algorithm.*

The results from trail testing can be corroborated with the results shown in Figure [4.5]. Results from the acceleration PSD plots do not indicate any appreciable difference as the damper current is increased from 0 to 1.4 A or in the two control algorithms, however the amplitude of the PSD of acceleration at the seat post is seen to reduce in all five cases.

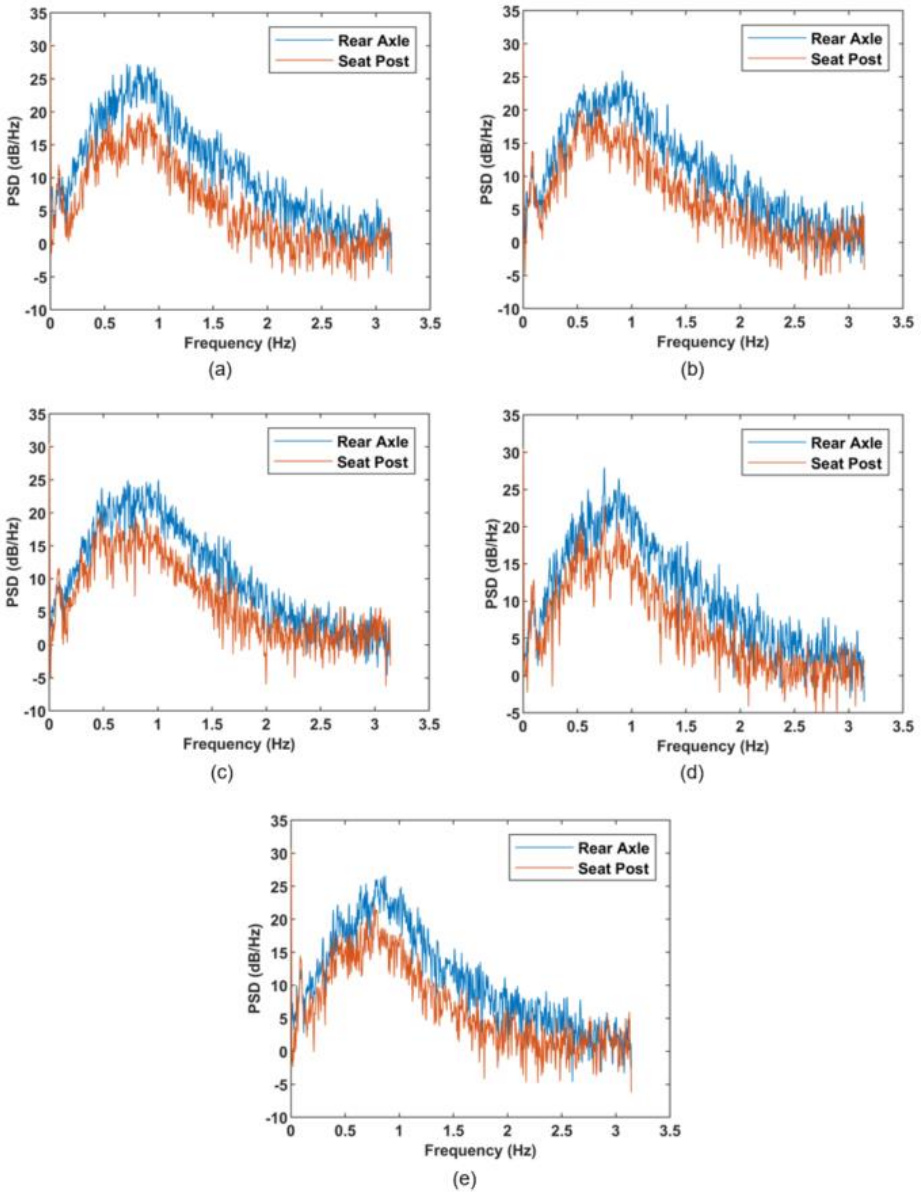


*Figure 4.5 - Power spectral density plots of acceleration data collected during trail testing. (a) Current = 0.0 A, (b) Current = 0.4 A, (c) Current = 1.4 A, (d) On/off control, (e) Proportional control.*

## 4.3 Mathematical Model Analysis

The mathematical model shown in Chapter 3, Figure [3.6], was used for preliminary analysis to understand the dynamics of a dual suspension bike mounted to a shaker table. The mass, stiffness and damping coefficient matrices of the mathematical model as well as data from a random road profile were analyzed and then plotted using the following types of plots:

1. Undamped Modes plot, Figure [4.6] - to determine the natural frequencies of the system and predict which frequencies would cause higher levels of vibrations.
2. Displacement Transmissibility plots, Figures [4.7-4.9] - to help identify natural frequencies of the system and determine how much vibration is transmitted to a specific part of the mountain bike from the source.
3. Power Spectral Density plots, Figures [4.10-4.12] - to quantify the strength of random vibrations (energy) as a function of frequency using a random road profile.

The boundary conditions used in these analyses are shown in Table [4.1 a and 4.1 b].

| Description | Symbol | Value |
|---|---|---|
| Distance between front and rear axle | b | 1.143 m |
| Distance between center of mass and rear axle | p | 0.381 m |
| Angle between ground and front fork | $\theta_1$ | 120 deg |
| Angle between ground and chain stay | $\theta_2$ | 0 deg |
| Angle between ground and seat stay | $\theta_3$ | 37 deg |
| Spring constant between front fork and frame | $k_f$ | 18000 N/m |
| Spring constant between front fork and ground | $k_{gf}$ | 1e8 N/m |
| Spring constant between seat stay / shock and frame | $k_r$ | 36000 N/m |
| Spring constant between seat stay / shock and ground | $k_{gr}$ | 1e8 N/m |
| Spring constant between chain stay and frame | $k_{L2}$ | 1e8 N/m |
| Distance between center of mass and axis of rotation | r | 0.762 m |
| Moment of Inertia of the Frame and Rider | I | 23.41 kg*m$^2$ |

*Table 4.2 a - Boundary Conditions for Mathematical Model*

| Description | Symbol | Value |
|---|---|---|
| Mass of the Frame and rider | m | 40.32 kg |
| Mass of the front fork | $m_f$ | 8.432 kg |
| Mass of the seat stay and shock | $m_r$ | 0.8775 kg |
| Mass of the chain stay | $m_{L2}$ | 0.0775 kg |
| Damping Current | w | 0.0, 0.4, or 1.4 Amps |
| Damping constant between front fork and frame | $c_f$ | 600 Ns/m |
| Damping constant between front fork and ground | $c_{gf}$ | 0 Ns/m |
| Damping constant between seat stay / shock and frame | $c_r$ | 15, 21.2, or 25.98 Ns/m |
| Damping constant between seat stay / shock and ground | $c_{gr}$ | 0 Ns/m |
| Damping constant between chain stay and frame | $c_{L2}$ | 0 Ns/m |
| Constant velocity | v | 4.5 m/s |

*Table 4.1 b - Boundary Conditions for Mathematical Model*

The values provided in Table [4.1 a and 4.1 b] were obtained by making measurements of a 2014 Specialized Epic mountain bike frame and by referring the published literature. To simplify the complexity of the system the values for $\theta_1$, $\theta_2$, $\theta_3$, and $c_r$ were all held constant. In reality, as the bike traverses a bump, the bike will pitch, and the shape of the rear triangle will change resulting in different angles for $\theta_1$, $\theta_2$, and $\theta_3$; however, the angles will change by less than 2 degrees. The

damping coefficient of the MR damper, which affects the $c_r$ value, is extremely complex. To simplify this value, three different $c_r$ values were determined using the RMS data collected from the shaker table analysis with a damper current set at 0.0, 0.4, and 1.4 amps. The $c_r$ values were determined to be 15, 21.2, and 25.98 Ns/m respectively. To mimic the shaker table set-up, the stiffness constants between the front fork and ground, rear axle and ground, and rear axle and frame via. the chain stay were set to 1e8 N/m to model them as being rigid; the corresponding damping constants were set to 0 Ns/m.

### 4.3.1 Undamped and Damped Modes

Two analyses were done to determine the modes of the system; one in which the system was undamped and another in which the system was damped. An analysis of the undamped system was used to simplify the problem and give a rough idea of the natural frequencies of the system and the vibration levels at specific points on the mountain bike. The damped system analysis was used to determine the natural frequencies and vibration levels of the system. Since the mathematical model had 7 DOFs there were 7 modes, or natural frequencies, for each case. Figure [4.6] shows the natural modes of the undamped system:

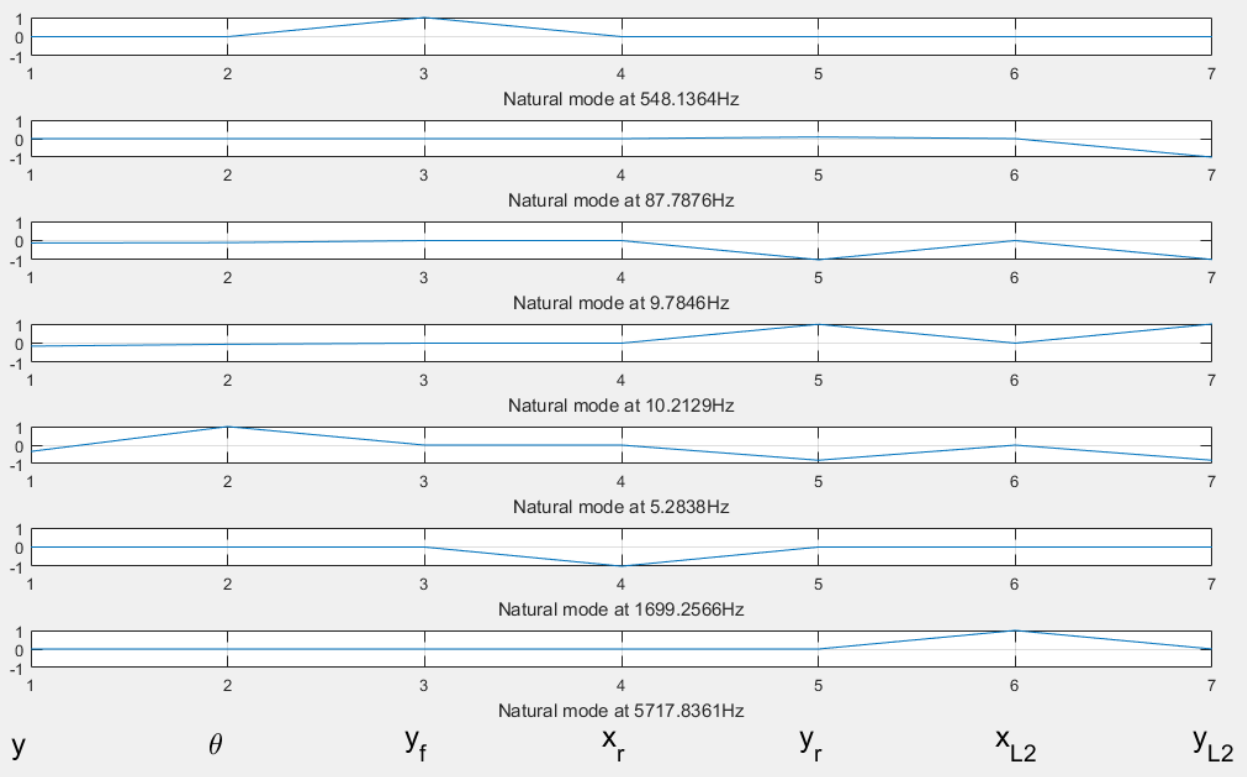


*Figure 4.6 - Natural Modes of the Undamped System*

Seven natural frequencies of the mathematical model were found to be located near 5.3, 9.8, 10.2, 88, 550, 1700, and 5700 Hz when the system is undamped. When damping is introduced to the system these natural frequencies change by less than 1 Hz. The following table displays which DOF were affected by the natural modes of the system:

| | | Natural Mode (Hz) | | | | | | |
|---|---|---|---|---|---|---|---|---|
| | | 5.3 | 9.8 | 10.2 | 88 | 550 | 1700 | 5700 |
| DOF | y | x | x | x | | | | |
| | θ | x | | | | | | |
| | $y_f$ | | | | | x | | |
| | $x_r$ | | | | | | x | |
| | $y_r$ | x | x | x | | | | |
| | $x_{L2}$ | | | | | | | x |
| | $y_{L2}$ | x | x | x | x | | | |

*Table 4.3 - Natural Modes for each DOF*

### 4.3.2 Transmissibility

The Transmissibility plot was used to identify where the natural frequencies are located and how much vibration is transmitted to a specific part of the mountain bike from the source. Transmissibility is the ratio of the maximum displacement of a specific point with the input displacement. A spike in the transmissibility plot indicates a possible natural frequency of vibration. Figures [4.7-4.9] are transmissibility plots for different sections of the bike. The different sections of the bike were plotted separately from each other so that the bike parts that are coupled are be plotted together. The 0-27.5 Hz range was selected to narrow the frequency bandwidth so that the relevant natural frequencies would be captured.

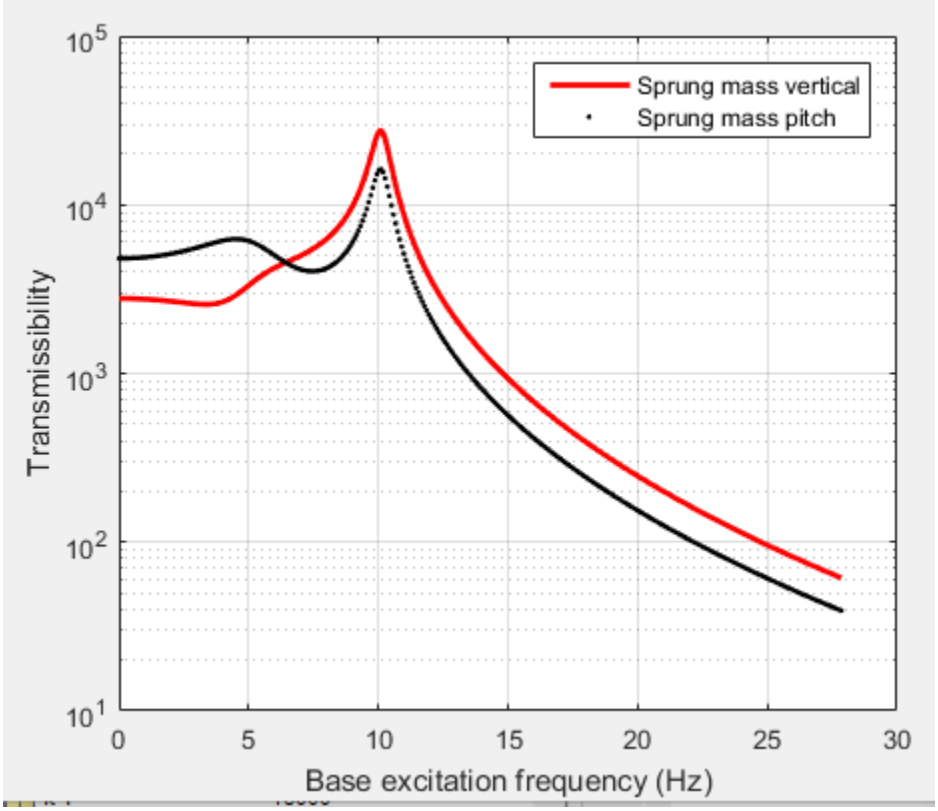


*Figure 4.7 - Transmissibility Plot (Sprung Mass Vertical and Sprung Mass Pitch)*

Figure [4.7] displays the comparison between the sprung mass vertical ($y$) to the sprung mass pitch ($\theta$). Examining the sprung mass vertical, it can be seen that there is a small response between 5-7 Hz and a much larger response around 10 Hz. The sprung mass pitch displays a strong response around 5 Hz and a large response near 10 Hz.

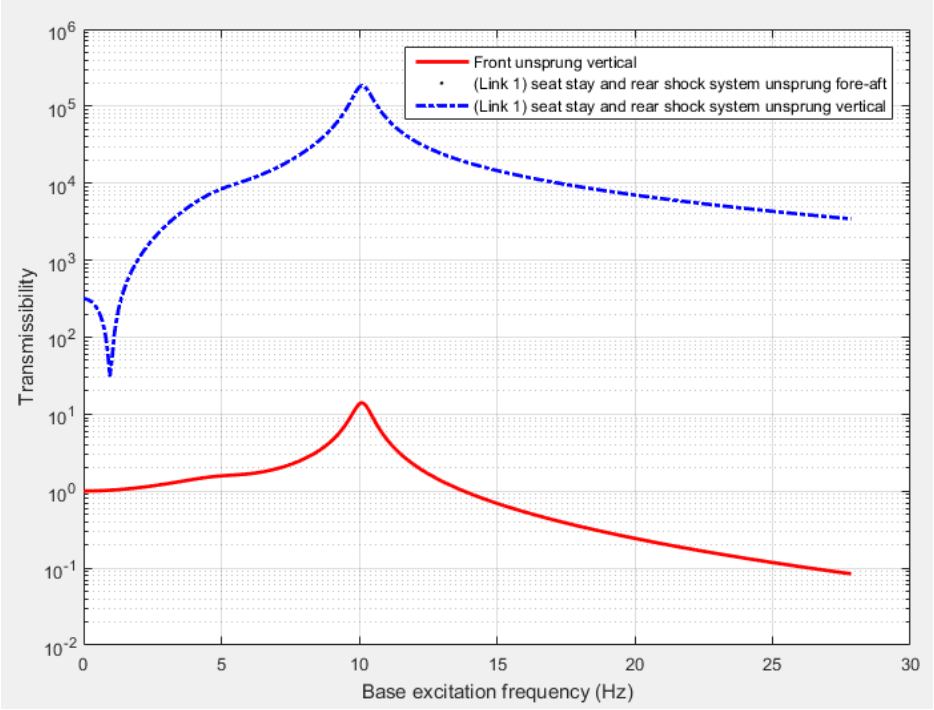


*Figure 4.8 - Transmissibility Plot (Front Unsprung Mass, Rear Shock and Seat Stay System Fore-aft, and Rear Shock and Seat Stay System Vertical)*

Figure [4.8] displays the comparison between the coupled system of the front unsprung vertical ($y_f$) to the rear shock and seat stay link system fore-aft ($x_r$) and the rear shock and seat stay link system vertical ($y_r$). The rear shock and seat stay link system fore-aft displays no change in transmissibility which is to be expected in this frequency range. The front unsprung vertical sees a small spike in the 5 and 9-11 Hz ranges. The rear shock and seat stay link system vertical sees a small response near 1 Hz, around 5 Hz and a large response between 9-11 Hz.

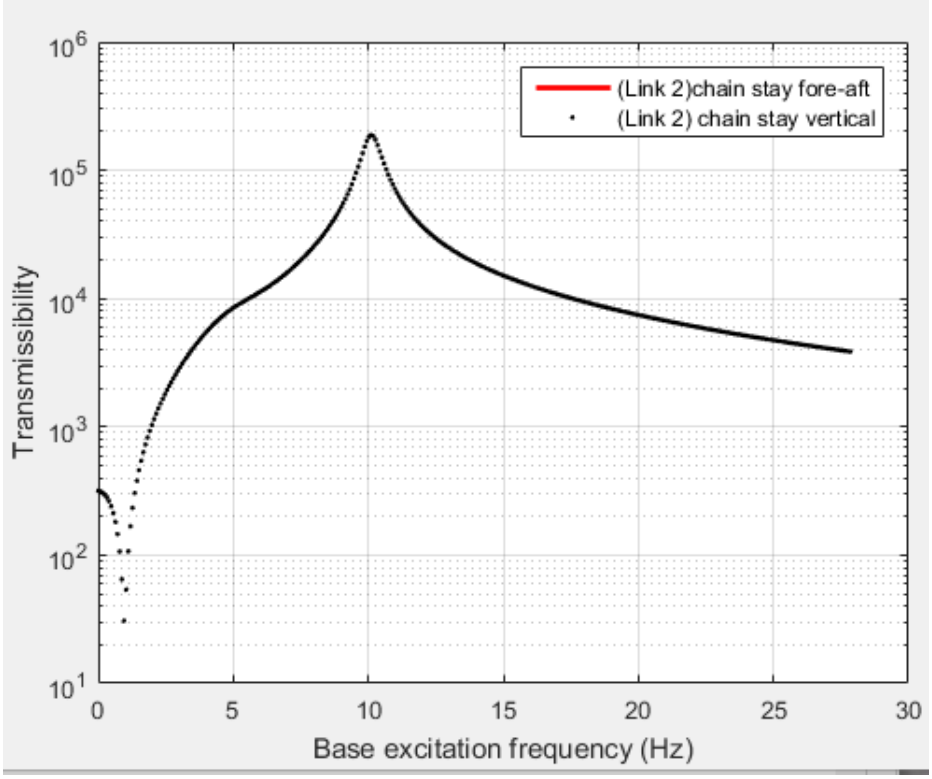


*Figure 4.9 - Transmissibility Plot (Chain Stay Fore-aft and Chain Stay Vertical)*

Figure [4.9] displays the comparison between the coupled system of the chain stay link fore-aft and the chain stay link vertical. The chain stay link fore-aft displays no change in transmissibility since the frequency range observed does not have an effect on this part of the bike. Similar to the rear shock and seat stay link system vertical, there are responses near 1, 5 and 9-11 Hz.

### 4.3.3 Power Spectral Density

The Power Spectral Density (PSD) plots were used to quantify the distribution of power caused by the vibration of a random road profile. In other words, PSD plots represent the energy in the system and will show which frequencies will have stronger vibration influence and which frequencies will have weaker influence on vibrations of the system. The PSD data from a good road surface was used with the bicycle traveling at a constant velocity of 4.5 m/s (about 10 mph). The "good" road surface is defined as being a smooth paved road with no cracks, bumps, turns, or elevation change. For future research, the good road surface will need to change such that it represents a good mountain bike trail surface. Using the PSD data from a good road surface, three PSD plots are displayed below comparing the sprung mass vertical ($y$) to the sprung mass

pitch ($\theta$) using a frequency range of 0-27.5 Hz, the front unsprung vertical ($y_f$) to the rear shock and seat stay link system fore-aft ($x_r$) and the rear shock and seat stay link system vertical ($y_r$) using the frequency range of 0-27.5 Hz, and the chain stay link fore-aft ($x_{L2}$) to the chain stay link vertical ($y_{L2}$) using the frequency range of 0-27.5 Hz. The 0-27.5 Hz range was selected to narrow down the frequency bandwidth such that the relevant natural frequencies would be captured.

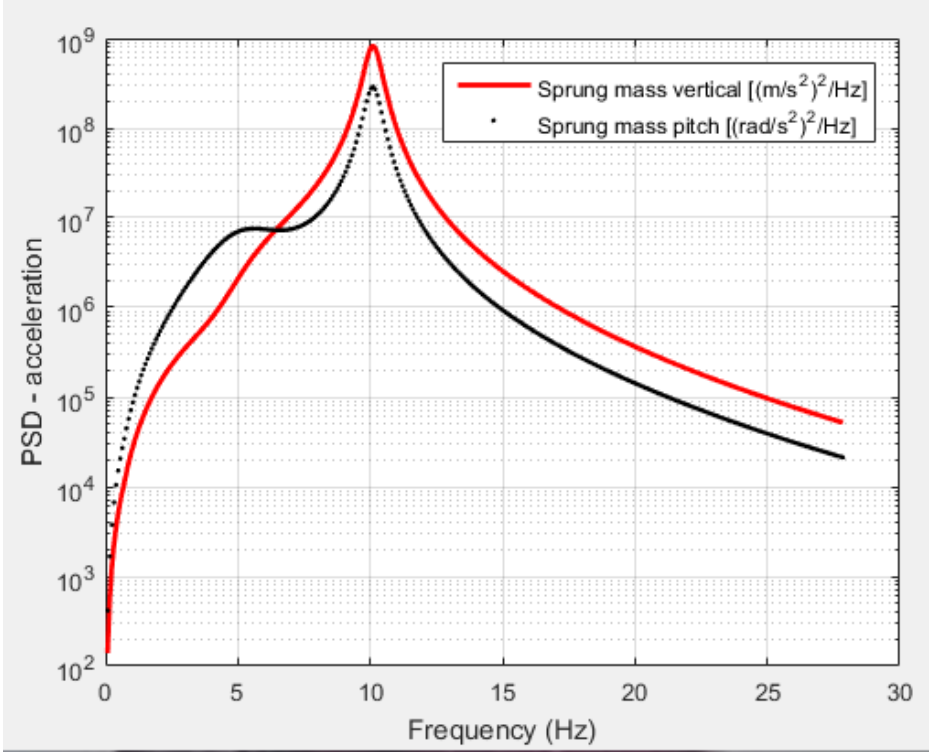


*Figure 4.10 - PSD Plot (Sprung Mass Vertical and Sprung Mass Pitch)*

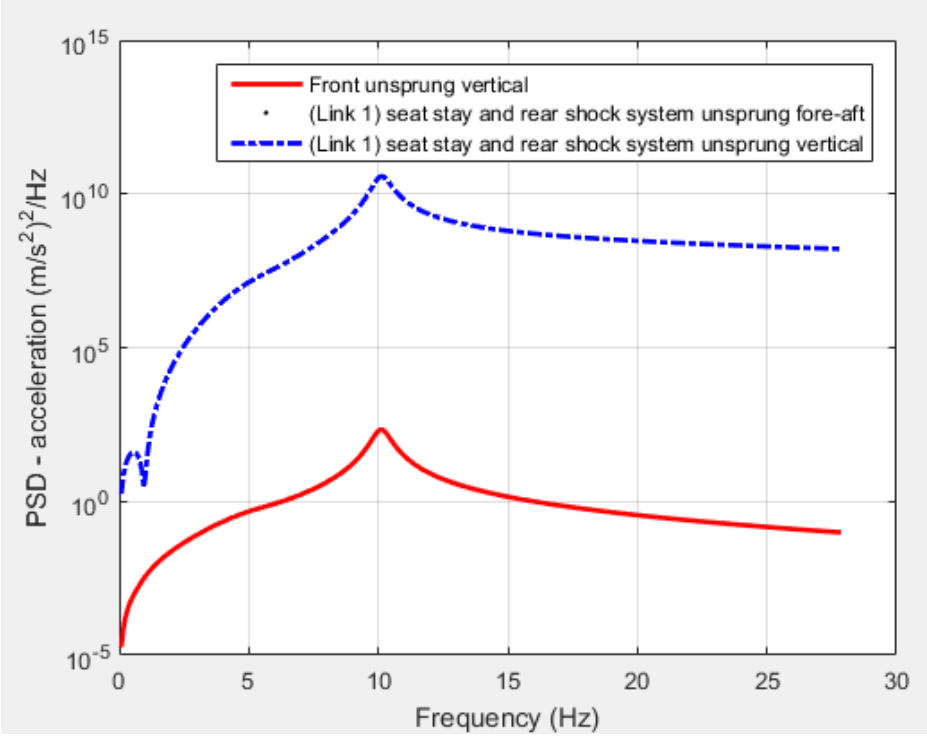


*Figure 4.11 - PSD Plot (Front Unsprung Mass, Rear Shock and Seat Stay System Fore-aft, and Rear Shock and Seat Stay System Vertical)*

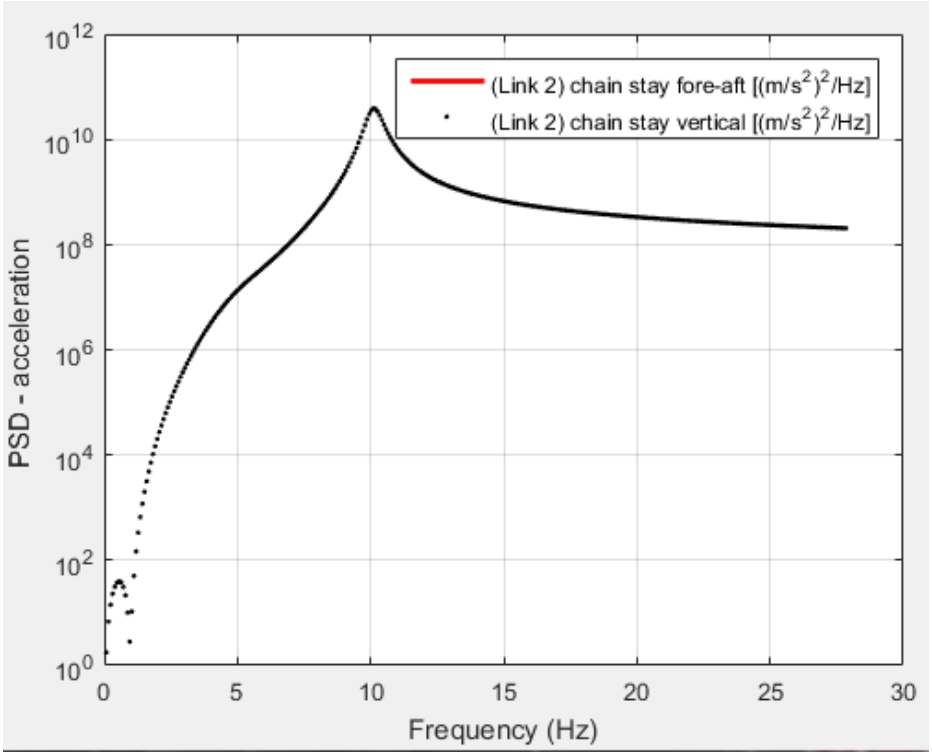


*Figure 4.12 - PSD Plot (Chain Stay Fore-aft and Chain Stay Vertical)*

Figures [4.10-4.12] display three different frequency bandwidths that excite the mountain bike; 0-1, 4-6, and 9-11 Hz. The excitation happening around 0-1 Hz effects the rear shock and seat stay system vertical as well as the chain stay vertical. The excitation happening around 5 Hz effects about half of the bike at different acceleration levels except for the front unsprung vertical, the rear shock and seat stay system fore-aft, and the chain stay fore-aft. The excitation happening around 9-11 Hz effects most of the bike at about the same acceleration levels except for the rear shock and seat stay system fore-aft and the chain stay fore-aft.

# CHAPTER FIVE: DISCUSSION

This chapter discusses the results obtained in the study, shows evidence of agreement and disagreement with past research, and summarizes the significance and practical importance of the results. Improvements for future testing are also mentioned in this chapter.

Before the tests were conducted the following assumptions were made to represent the bicycle and collect the data. For the shaker table test, weights were distributed at each handlebar and the seat post to represent the rider; where the majority of the weight was located at the seat post and the weight at each handlebar represented the rider's hands and arms. The bicycle was also mounted to the fixed frame structure via. the lower bracket to represent the weight of the rider's legs and feet. The data was collected in the z-axis (perpendicular to the ground) only since it was assumed that the rider and bicycle were traveling in a straight line at a constant velocity. The mathematical model was modeled to represent the shaker table test by using the governing equations of motion. The model was assumed to be and in-plane model to capture the dynamics of the bicycle while traveling in a straight line. The model was divided into four rigid bodies to represent the mountain bike such that link 1 and the rear shock system were combined into one rigid body and link 3 was not modeled. This assumption was made since the purpose of link 3 is for kinematics such that it is designed to keep link 1 and the rear shock system linear to each other. During the analysis the rear axle and front fork axle where represented as being rigidly mounted they are both rigidly mounted to the shaker table and fixed frame structure. Finally, since the MR damper characteristics are complex, the damping coefficient for the rear shock system was determined by using the data from the shaker table test and set to a single value.

### 5.1 Shaker Table

During the shaker table testing two types of plots were used to analyze the data; RMS and Frequency Response. The RMS (root mean square) plots were used to capture meaningful and effective acceleration values of different tests and compared to each other. The test run at 2 Hz behaved as expected; as the current is increased the shock absorber becomes stiffer and the acceleration at the saddle increases. The frequency response plots were used to provide insight into the systems dynamics, such as frequency-dependent gains, resonances, and phase shifts. At 2 Hz, increasing the damper stiffness increases the relative magnitude of the response at the seat post but the frequencies that are excited do not change. This indicates that at a relatively low frequency, it may be possible to control the response of the shock absorber by using a proportional control algorithm.

The test run at 5 Hz acted in a different manner; as the current was increased and the shock absorber became stiffer, the acceleration at the saddle dropped initially and then increased significantly. The frequency plots at 5 Hz and for the sine sweep input of 1-20 Hz also show an increase in the magnitude of the response at the seat post as the damper current is increased. This type of response could be that there is a natural frequency of the system located near the 5 Hz resonance. The evidence for this natural frequency is strengthened by the results of the mathematical model, where a natural frequency was calculated to be near 5 Hz.

At the higher input frequencies of 10 and 20 Hz, changes in the damper stiffness do not appear to have much effect on the response of the bike at the seat post. These results would suggest that at higher frequencies changing the current input to the MR damper would not change the response at the saddle significantly. The frequency plots for the sine sweep of 1-20 Hz do not indicate any additional natural frequencies in the tested bandwidth. However, the

mathematical model results indicate that two additional natural frequencies should have been observed in the 1-20 Hz bandwidth near 10 Hz. These two additional natural frequencies observed in the mathematical model analysis could indicate that further adjustments are needed to be applied to the model to better represent the shaker table test. On the other hand, the shaker table results may not have registered the other two natural frequencies due the system having an additional pathway to ground. This additional pathway to ground would almost certainly induce frame accelerations making it more difficult to isolate the effects of the rear shock.

### 5.2 Trail System

The results for the trail tests were unexpected given the response received from the shaker table testing. The results showed some variation in the data with the changing current but there did not seem to be a clear effect of changing the damping current on the acceleration at the seat post. The on/off and proportional control algorithms both demonstrated a significant reduction in the acceleration at the seat post. Based on the results for the trail test a clear distinction cannot be made between the responses at different damper currents and the two control algorithms. This could be due to the range of frequencies that were excited on the mountain trail as compared to the shaker table, where only a single input frequency was applied. Future trail testing should be conducted to reach input frequencies higher than 3 Hz.

### 5.3 Mathematical Model

The mathematical model results were analyzed using undamped mode plots, displacement transmissibility plots, and PSD plots. The undamped and damped mode plots show seven natural modes of vibration at frequencies of 5, 9.8, 10.2, 88, 550, 1700, and 5700 Hz. The natural modes at 88, 550, 1700, and 5700 Hz were not considered for this study. These higher order modes were not considered for this study due to inaccuracies associated with the numerical

computation of higher order modes. Furthermore, since high stiffness values have been used to represent rigidity of some of the links, higher order modes may not accurately represent the dynamics of the system. The natural modes at 5, 9.8 and 10.2 Hz can be processed and have been further analyzed using transmissibility and PSD plots to determine the bicycle characteristics at these given frequencies. The future development of the damper should primarily focus on the lower natural modes at 5, 9.8, and 10.2 Hz to reduce the magnitude of vibrations felt at these frequencies since the excitation frequency over a bumpy trail is typically below 5 Hz but could potentially reach 10 Hz. Some consideration should be taken for the higher natural modes at 88, 550, 1700, and 5700 Hz since low input frequencies could still excite higher-order vibration modes. The undamped system simulation is used as a baseline and was followed by the analysis of the damped system. The natural frequencies of the damped system varied from those of the undamped system by less than 1 Hz.

The mode shapes in Figure [4.6] have been scaled to a maximum magnitude of $\pm 1$, and the numbers in the *x*-axis correspond to the seven DOF. The natural modes imply that for excitation input due to irregularity of the random road profile, the lowest natural mode will be excited at 5 Hz and the highest mode will be excited at 5700 Hz. Incorporating the damping constants yields the damped frequency as well as the damping ratios for each mode. These results are summarized in Table [5.1].

| Undamped Frequency (Hz) | Damped Frequency (Hz) | Damping Ratio | Mode Shape |
|---|---|---|---|
| 5.28 | 5.01 | 0.339 | Sprung mass vertical, sprung mass pitch, seat stay and rear shock vertical and chain stay vertical |
| 9.78 | 9.51 | 0.287 | Sprung mass vertical, seat stay and rear shock vertical and chain stay vertical |
| 10.21 | 10.11 | 0.034 | Sprung mass vertical, Seat stay and rear shock vertical and chain stay vertical |
| 87.79 | 87.21 | 0.115 | Seat stay and rear shock vertical and chain stay vertical |
| 548.14 | 548.08 | 0.009 | Front unsprung vertical |
| 1699.26 | 1699.25 | 0.004 | Seat stay and rear shock fore-aft |
| 5717.84 | 5717.81 | 0.001 | Chain stay fore-aft |

*Table 5.1 - Mode Shapes and the Corresponding Damping Characteristics*

The mathematical model shows a natural mode near 5 Hz corresponding to the bounce and pitch of the frame/rider degree-of-freedom. This mode was directly measured through shaker table testing by the accelerometer at the seat post. Therefore, it can be concluded that the mathematical model correctly represents the overall dynamics of the bicycle pertaining to the sprung mass. However, the mathematical model shows two modes at 9 and 10 Hz primarily pertain to the vertical motion of Link 1 and Link 2 with some limited coupling to the sprung mass bounce. The test data does not show these two modes since these two modes are not directly coupled to the sprung mass and, therefore, may not be seen in the measurement at the sprung mass. This can also be seen from the transmissibility results.

The undamped and damped modes were used to analyze the transmissibility due to excitations introduced to the rear axle. Figures [4.7-4.9] show the transmissibility of the sprung mass and the front and rear unsprung masses due to excitation at the rear axle. In Figure [4.7], the sprung mass vertical and sprung mass pitch both display a large response throughout the 0-27.5 Hz bandwidth with an additional spike at 10 Hz. The sprung mass pitch also has a sizable spike at 5 Hz and the sprung mass vertical has an additional spike near 7 Hz. The magnitude of

the overall response could be attributed to the rigid mount between the rear axle and the shaker table platform. The stiffness constant between these components is 1e8 N-m. If this were modeled such that the tire was mounted to the bike and rested on the shaker table platform the magnitude of the overall response would be reduced. Based on the model analysis, the magnitude of the response found for both the sprung mass vertical and sprung mass pitch near 10 Hz could be attributed to the seat stay and rear shock vertical and the chain stay vertical. These components experience a large response at the 9.8-10.2 Hz resonance.

Figure [4.8] shows the transmissibility of the front unsprung vertical, the seat stay and rear shock vertical, and the seat stay and rear shock fore-aft. The seat stay and rear shock vertical displays a large response throughout the 0-27.5 Hz bandwidth as well as two spikes located near 0 and 10 Hz. The magnitude of the overall response could be attributed to the rigid mount between the rear axle and the shaker table platform. The response seen at 5 and 10 Hz are due to the natural modes located at these frequencies which excite this part of the bicycle. The response near 0 Hz is unusual and warrants further investigation since an object having a natural mode at 0 Hz would not have a long lifespan, which is not the case for bicycles. The front unsprung vertical shows a small response near 5 Hz and a large response near 10 Hz. It is not clear where these responses are coming from since this part of the bike should only see a large response when the bicycle is excited near 550 Hz. However, one possible cause is that the transmissibility of other regions of the bicycle may be large enough at the lower frequencies that they are affecting the transmissibility of this portion of the bicycle. The seat stay and rear shock fore-aft does not display any response at these lower frequencies which is expected since the mode that excites this part of the bicycle is at 1700 Hz. The seat stay and rear shock fore-aft having no

response could also be caused by the rear axle having a rigid mount to the shaker table platform which only moves in the y-axis and not the x-axis.

Figure [4.9] shows the transmissibility of the chain stay vertical and the chain stay fore-aft. As can be seen from Figure [4.9], the chain stay vertical displays a large response throughout the 0-27.5 Hz bandwidth with additional spikes near 0, 5, and 10 Hz. The magnitude of the overall response could be attributed to the rigid mount between the rear axle and the shaker table platform. The response seen at the 5 and 10 Hz are due to the natural modes located at these frequencies. Similar to the seat stay and rear axle vertical the response seen near 0 Hz warrants further investigated. The chain stay fore-aft does not display any response at these lower frequencies which is expected since the mode that excites this part of the bicycle is at 5700 Hz. The lack of response could also be caused by the pin connection between the rear axle and the shaker table. Examining Figures [4.8 and 4.9], the seat stay and rear shock and the chain stay seem to have almost identical responses. This could be due to the fact that both links receive the same excitation and displacement where they are joined at the rear axle.

The transmissibility results suggest that using the pin joint to attach the rear axle to the shaker table platform creates excessively high displacements throughout the bicycle. In future experiments, it might be advisable to remove this pin joint.

The PSD plots, seen in Figures [5.10-5.12], display similar results to the transmissibility plots where some of the bicycle parts are coupled together and experience responses at the same frequencies. The difference between the two plots are that the transmissibility plots show what frequencies excite displacement whereas the PSD plots show what frequencies excite high levels of energy. The frequencies at which a response was seen in the transmissibility plots correspond to the same frequencies where responses are seen in the PSD plots. The only variance between

the frequencies that show a response between the transmissibility and PSD plots correspond to the seat stay and rear shock vertical and the chain stay vertical. These two display a response near 1 Hz. The results associated with Link 1 and Link 2 that show a local peak near 1 Hz do not correspond to a natural frequency but might represent some coupled modes between Link 1, Link 2 and other rigid bodies. This could be investigated further by modifying some of the modeling assumptions and collecting acceleration data at multiple locations on the bike.

### 5.4 Suggested Improvements to the Experimental Methods

After conducting the shaker table experiment, three modifications to the shaker table set-up could improve the experiment and better represent a mountain bike on a mountain trail. First, adjusting the frame structure such that it is mounted to the shaker table so that there is only one path to ground. The existence of multiple ground paths almost certainly induces frame accelerations that make it more difficult to isolate the effects of the rear shock. Second, removing the mount at the bottom bracket axle would be a better representation of a mountain bike on a trail. Removing this mount will allow the mountain bike to translate perpendicular to the ground and allow the chain stay link to influence the vibration effects of the bicycle. By removing this mounting joint, the bike may become unstable and move out of plane. If stability is an issue after removing this mount, then the frame could be stabilized using other methods found in literature such as using bungee cords. Finally, removing the rigid mount at the rear axle, reattaching the rear wheel, and running the test such that the rear wheel is resting on the shaker table platform. This would allow the bicycle to bounce freely as it would when riding on a mountain trail. It would also allow inclusion of displacement and damping of the wheel and tire.

# CHAPTER SIX: CONCLUSION AND FUTURE RESEARCH

A review of the current literature in mountain biking reveals that there is a need for development in the rear shock system to balance the need for pedaling efficiency with comfort and trail contact. While multiple semi-active rear shock systems exist, they only operate using an on/off control algorithm. This thesis has presented experimental and analytical research into the use of an MR damper to implement a range of damping levels. This work forms a basis for further investigation into the use of control algorithms that contain a proportional term.

The principle goal of this research was to characterize the dynamics of a mountain bike that utilizes an MR damper-based rear suspension. Three primary research questions were addressed:

1. Can a mountain bike rear shock absorber be designed to utilize a MR damper with a control algorithm that is more complex than a simple on-off controller?
2. How does changing the shock control algorithm affect the performance of the mountain bike?
3. Can a mathematical model be formulated that captures the dynamics of the mountain bike?

This study has provided the detailed design of a shock absorber for a mountain bike that utilizes an MR damper. The rear shock absorber consisting of commercially available air springs and MR damper has been installed in a 2014 Specialized Epic “cross-country” style mountain bike. Two experiments were used to evaluate the damper using a shaker table as well as on a mountain trail. On/off control and proportional control algorithms have been implemented to provide active damping which can be controlled through a feedback control system that is

implemented on a microcontroller and utilizes acceleration input from a MEMS accelerometer mounted at the rear axle of the bike. Since the control algorithm is implemented in the microcontroller program, it can be easily modified to accommodate a different logic for ride comfort or bike handling. The rear suspension system has also been designed such that it can be used as a baseline to develop different control algorithms that can be used to tailor the response of the bike to different trail conditions and ride requirements.

Experimental results from the shaker table indicate that the response of the bike frame to input frequencies in the 0-5 Hz range can be controlled by controlling the current to the MR damper. This is useful in mountain biking since the excitation frequency over a bumpy trail is typically below 5 Hz. The experimental results with the input frequencies in the 10-20 Hz range indicate that there is little to no affect or correlation between changing the input current to the damper to the seat post isolation even though the system still exhibits ride comfort by mitigating acceleration transmitted from the rear wheel.

To test the bike on a mountain trail, the experiment was modified so that it was portable. In addition to the constant damper current approach, on/off and proportional control algorithms were implemented. Both control algorithms demonstrate significant reduction of acceleration at the seat post, however the data acquired using each of the two algorithms was not significantly different. Investigation of more advanced control algorithms is a direction for future work.

After testing the MR damper-based shock absorber on the shaker table and mountain trail experiments, a mathematical model of the shaker table experiment was designed such that it could be used for preliminary analysis to understand the dynamics of a dual suspension mountain bike mounted to a shaker table. Upon the analysis using MATLAB, three frequencies, located near 5, 9 and 10 HZ, were found to be natural modes of the system that transmit large amounts of

energy from one body of the system to another. Since the shaker table data only found a natural mode near 5 Hz, the mathematical model should undergo additional modifications in order to better represent the shaker table test. However, modeling the bicycle as a mass spring damper system adequately represented the shaker table testing method.

The scope of research carried out in this study can be enhanced to gain a greater understanding of how the MR damper functions and improves the capabilities of the rear suspension of a mountain bike. The future work of this study could focus on the following four concepts:

1. Changing the bike mounting approach on the shaker table to remove the pin joint and multiple grounds.
2. Develop a random trail profile that can be programmed into the shaker table.
3. Development of more complex control algorithms that use a proportional control term.
4. Development of a rear shock that has a size and weight similar to existing shocks.

As discussed in the discussion chapter, suggested improvements to the experimental methods, changing the bike mounting approach on the shaker table to remove the pin joint located at the bottom bracket would help in better representing the bike as if it were on a mountain trail. Removing multiple grounds to the system, until there is only one, would apply better engineering and vibration standards, such that there would not be additional accelerations induced to the frame. Having the one pathway to ground would allow the effects of the rear shock to be easily isolated.

The second way to gather more meaningful data is by developing a random trail profile that can be programmed into the shaker table. This would allow experiments to be performed under more controlled and repeatable conditions than testing on an actual trail. This would also

allow for experiments to be performed in-house with a large customable range of tests that could simulate a variety of trail conditions. It should be noted that actual testing on mountain trails should still be conducted to test the rear shock system performance.

As more tests are run at different frequencies, input currents, and random trail profiles, the control algorithm that uses a proportional control term would have the capability to become more complex. These additional tests would provide specific acceleration data on how the rear shock system influences the vibrations at the saddle at every frequency tested when applying each incremental damping constant. With this data, the user could program a complex control algorithm such that they could optimize how the bike will respond to input accelerations at the rear wheel.

The final improvement that could further advance the rear shock system is to develop the rear shock such that it has a size and weight similar to existing shocks. The current shock system did not take into the consideration of size and weight since it was intended for experimental use only. The biking industry spends a lot of time and money in the development of bicycles that weigh less. It is their belief that reducing the weight of a bicycle by even a few ounces can provide the competitive edge desired by experience riders.

To conclude the research done so far on the implementation of a magnetorheological damper for active vibration isolation and performance of a mountain bike rear suspension the following conclusions can be made:

1. Tests done on the shaker table indicate that for relatively low frequencies, it may be possible to control the response of the shock absorber by using a proportional control algorithm.

2. The trail tests concluded that a clear distinction cannot be made between the responses at different damper currents and the two control algorithms. However, this could be due to the range of frequencies that were excited on the mountain trail as compared to the shaker table, where only a single input frequency was applied.
3. Both the on/off and proportional control algorithms demonstrate significant reduction of acceleration at the seat post, however the data acquired using each of the two algorithms was not significantly different. Investigation of more advanced control algorithms is a direction for future work.
4. Upon the analysis using MATLAB, the mathematical model it correctly represented the overall dynamics of the bicycle pertaining to the sprung mass. Additional accelerometers will need to be placed throughout the bicycle to determine if the mathematical model correctly represented the overall dynamics of the bicycle as a whole.

# REFERENCES


[1] Brain Technology. (n.d.). Retrieved from https://www.specialized.com/us/en/stories/brain-technology

[2] Wang, J., & Meng, G. (2001). Magnetorheological fluid devices: Principles, characteristics and applications in mechanical engineering. *Proceedings of the Institution of Mechanical Engineers, Part L: Journal of Materials: Design and Applications*, *215*(3), 165–174.

[3] Faiss, R., Praz, M., Meichtry, A., Gobelet, C., and Deriaz, O. The Effect of Mountain Bike Suspensions on Vibrations and Off-Road Uphill Performance, *Journal of Sports Medicine and Physical Fitness*, 47, 151-158, (2007).

[4] Champoux, Y. & Richard, S. & Drouet, J.-M. (2007). Bicycle structural dynamics. Sound and Vibration. 41. 16-24.

[5] Koellner, A., Cameron, C., Battley, M., 2014. Measurement and analysis system for bicycle field test studies. Proceedings of Engineering of Sport Conference 10 (Procedia Engineering), Sheffield, United Kingdom, 10-14.07.2014.

[6] Lépine, J., Champoux, Y. & Drouet, J. A Laboratory Excitation Technique to Test Road Bike Vibration Transmission. *Exp Tech* 40, 227–234 (2016). https://doi.org/10.1007/s40799-016-0026-8

[7] A. N. Thite, S. Gerguri, F. Coleman, M. Doody & N. Fisher (2013) Development of an experimental methodology to evaluate the influence of a bamboo frame on the bicycle ride comfort, Vehicle System Dynamics, 51:9, 1287-1304, DOI: 10.1080/00423114.2013.797591

[8] Farrel, P. The Roots of Dirt: How Mountain Bikes Went from Clunkers to Global Phenomenon, Wired, www.wired.com/2016/06/history-mountain-bike-unsurprisingly-badass/, (Retrieved on June 4, 2016).

[9] Rome, D. Fox Live Valve Suspension: The Future is Now, Cyclingtips, Retrieved from https://cyclingtips.com/2018/08/fox-live-valve-electronically-controlled-suspension/, (Accessed August 29, 2018).

[10] Batterbee, D. C., and Sims, N. D. Magnetorheological platform dampers for mountain bikes, *Proc. SPIE 7290, Industrial and Commercial Applications of Smart Structures Technologies*, 72900B, (2009).

[11] Breese, D. G., and Gordaninejad, F. Semiactive field-controllable magneto-rheological fluid dampers for mountain bicycles, *Proc. SPIE 3991, Smart Structures and Materials 2000: Industrial and Commercial Applications of Smart Structures Technologies*, (2000).

[12] Poynor, JC (2001) Innovative designs for magneto-rheological dampers. MS Thesis, Virginia Polytechnic Institute and State University, Blacksburg, VA.

[13] Kaul, S. Recursive Modeling of a Magneto-Rheological Damper, *International Journal of Mechanical and Materials Engineering*, 6, 31-40, (2011).

[14] Meeser, R. F., Kaul, S., and Els, P. S. Investigation into the Flow-Blocking Ability of a Novel Magneto- Rheological Damper Unit, *ASTM Journal of Testing and Evaluation*, 45, 1601-1608, (2017).

[15] Nielens, H., and Lejeune T., Energy Cost of Riding Bicycles with Shock Absorption Systems on a Flat Surface, *International Journal of Sports Medicine*, 22, 400-404, (2001).

[16] MacRae, H., Hise, K., and Allen, P. Effects of Front and Dual Suspension Mountain Bike Systems on Uphill Cycling Performance, *Medicine and Science in Sports & Exercise*, 32, 1276-1280, (2000).

[17] Nielens, H., and Lejeune, T. Bicycle Shock Absorption Systems and Energy Expended by the Cyclist, *Sports Medicine*, 34,71-80, (2004).

[18] Williams, T., Kaul, S., and Dhingra, A. Influence of Frame Stiffness and Rider Position on Bike Dynamics: Analytical Study, *Proc. ASME International Mechanical Engineering Congress and Exposition*, IMECE 2015, Houston, TX, (2015).

[19] S. Kaul, Influence of a Vibration Isolation System on Planar Dynamics of a Motorcycle, International Journal of Acoustics and Vibration, Vol. 25, No. 1, pp. 96-103, 2020.

[20] McAndrews, M. Bicycle Shock Absorber with Slidable Inertia Mass, United States Patent 8,960,389.

[21] Carlson, J. D. MR Fluids and Devices in the Real World, *International Journal of Modern Physics B*, 19, 1463-1470, (2005).

[22] L. Sun, On Human Perception and Evaluation to Road Surfaces, *Journal of Sound and Vibration*, 247, 547-560, (2001).

[23] R. Pierce, S. Kaul, J. Friesen, T. Morgan, Mountain Bike Rear Suspension Design: Utilizing a Magnetorheological Damper for Active Vibration Isolation and Performance. "*Journal of Acoustics and Vibrations* (submitted)."